points (see Fig. 2A), and used in ELISA analysis and in the in vitro neutralization assay described below. All animal experiments using rabbits were approved by The Tokyo Metropolitan Institute of Medical Science Animal Experiment Committee and were performed in accordance with the animal experimentation guidelines of The Tokyo Metropolitan Institute of Medical Science.

ELISA

Recombinant SARS-CoV N, M, E, and S proteins tagged with six histidines at the C terminus were expressed in RK13 cells by infecting with mOrVV-N-His, mOrVV-E-His, mOrVV-M-His, or mOrVV-S-His at an MOI of 5. These proteins were purified using nickel Sepharose (6 Fast Flow; GE Healthcare). His-tagged E and M proteins were further purified by SDS-PAGE. These full-length structural proteins (0.2 μg/ml, 50 μl/well) were coated onto 96-well plates at 4°C overnight. The plates were blocked with 1% BSA in PBS(−) that contained 0.5% Tween 20 and 2.5 mM EDTA, and then incubated with serial 2-fold dilutions of sera from the rabbits immunized with m8rVV-NMES or m8. After extensive washing, the plates were assayed as previously described, except that *o*-phenylenediamine was used as the substrate (17). The individual SARS-CoV structural protein-specific IgG titers are presented as the end point dilution Ab titers. The end point titer was defined as the reciprocal of the highest dilution of serum at which the absorbance at 490 nm (A_{490}) ratio (A_{490} of m8rVV-NMES-immunized serum/A_{490} of m8-immunized serum (negative control)) was greater than 2.0, as previously described (19).

In vitro neutralization assay for SARS-CoV

The neutralizing Ab titers of the sera of rabbits immunized with m8rVV-NMES or m8 were determined as previously described (17). Briefly, serial 2-fold dilutions of heat-inactivated sera were mixed with equal volumes of 200 tissue culture ID_{50} ($TCID_{50}$) of SARS-CoV and incubated at 37°C for 1 h. Vero E6 cells were then infected with 100 μl of the virus-serum mixtures in 96-well plates. After 5 days (or 6 days in the SARS-CoV challenge experiment) of infection, the neutralization titer was determined as the end point dilution of the serum at which there was 50% inhibition of the SARS-CoV-induced cytopathic effect. The method used for end point calculation was that described by Reed and Muench (20).

SARS-CoV challenge experiment

Female BALB/c mice older than the 6 mo of age (SLC) were used in this study. Four groups of eight BALB/c mice (seven mice in the vehicle-immunized group) were inoculated intradermally with either 1×10^7 PFU/body of m8, m8rVV-S, or m8rVV-NMES or 70 μl of vehicle (MEM without FCS). At 7–8 wk postimmunization, the mice were infected intranasally with 1×10^5 $TCID_{50}$/body of SARS-CoV (20 μl/mouse), as previously described (11). Four mice from each group were sacrificed 2 and 9 days later, except for the three mice of the vehicle-immunized group, which were sacrificed 2 days later. The mice were sacrificed under anesthesia and the lung, liver, small intestine, and spleen were extirpated. Aliquots of these tissues were frozen immediately at −80°C or fixed with 10% formalin. The collected blood was used for the in vitro neutralization assay. In addition, BALB/c mice were injected intradermally with 1×10^7 PFU/body of recombinant VV that expressed each structural protein of SARS-CoV (mOrVV-NHis, mOrVV-MHis, mOrVV-EHis, mOrVV-SHis) with or without LC16mOrVV-SHis (i.e., LC16mOrVV-N, -M, -E, -S alone or LC16mOrVV-N + LC16mOrVV-S, -M + LC16mOrVV-S, or -E + LC16mOrVV-S), and infected with 1×10^5 $TCID_{50}$/body of SARS-CoV more than 4 wk later. After 2 and 9 days, mice (n = 3–5 per group) were sacrificed following blood collection under anesthesia, and their lungs were extirpated. All animal experiments using mice were approved by the Animal Experiment Committee at The Institute of Medical Science, University of Tokyo, and were performed in accordance with the animal experimentation guidelines of The Institute of Medical Science, University of Tokyo.

Determination of viral titers in the organs

The SARS-CoV titers in the mouse organs were determined as previously described (11). Briefly, tissue samples (i.e., lung, liver, small intestine, and spleen) were homogenized in a 10-fold volume of Leibovitz 15 medium (Invitrogen). The homogenates were centrifuged at 2000 rpm for 10 min at 4°C. Serial 10-fold dilutions of the supernatants of these homogenates were added to Vero E6 cells seeded on 96-well plates. After 6 days of incubation, the cells were fixed with 10% formalin. Viral titer was determined as the 50% end point dilution of the homogenate that induced the cytopathic effect. The method used for end point calculation was that described by Reed and Muench (20).

Lung histopathology and inflammation scores

In accordance with a previous report (11), 10% formalin-fixed lung tissues of the SARS-CoV-infected mice were embedded in paraffin. Paraffin block sections (4-μm thickness) were stained with H&E staining. The peribronchial and perivascular scores were recorded in a blinded fashion by a pathologist. We evaluated pulmonary pathology using the histopathologic scoring systems developed by Cimolai et al. (21), in which the scoring system is weighted heavily for bronchial lesions. This scoring system allowed us to differentiate the severity of pulmonary pathology in small groups of animals. The pathology grading system consisted of a numerical score ranging from 0 to 26. In brief, each section was scored based upon a cumulative total from five categories that incorporated evaluations of the following: A) number of bronchiolar and bronchial sites affected by the periluminal infiltrate (range, 0 to 3); B) severity of the periluminal infiltrate (range, 0 to 3); C) luminal exudate severity (range, 0 to 2); D) frequency of perivascular infiltrate (range, 0 to 3); and E) severity of parenchymal pneumonia (range, 0 to 5). The accumulated numeric score was derived from the sum of the subscores: A+3(B+C)+D+E. Eosinophils were detected in tissue sections by method of Luna (22).

Extraction of total RNA and quantitative RT-PCR of cytokine or chemokine mRNA

To measure the levels of cytokine or chemokine mRNA, total RNA samples were extracted from the lungs using the RNeasy Mini kit (Qiagen). Quantitative RT-PCR was conducted with TaqMan Gene Expression assays (Applied Biosystems) using the ABI Prism 7700 and Sequence Detection System software v.1.7. The fold change in copy number of each cytokine/chemokine mRNA was revealed using the $2^{-\Delta\Delta C_t}$ method using 18 S rRNA as an endogenous calibrator.

Statistical analysis

Data are presented as mean ± SD. Statistical analysis was performed by one-way ANOVA, followed by the Dunnett or Bonferroni test. A value of $p < 0.05$ was considered to be statistically significant.

Results

Generation of recombinant VV that expresses the structural proteins of SARS-CoV

A multicistronic transgene that expresses simultaneously four structural proteins (N, M, E, and S proteins) of SARS-CoV was constructed and inserted into the HA locus of LC16m8 (m8) by homologous recombination (Fig. 1*A*). Expression of the transgene was placed under the control of the powerful ATI/p7.5 hybrid promoter. We screened for m8rVV-NMES using the erythrocyte agglutination assay (17), and confirmed the insertion of the transgene by PCR. Expression of the N, M, E, and S proteins in Vero E6 cells infected with m8rVV-NMES was detected by Western blot analysis. Recombinant LC16mO (mO) expressing the C-terminal histidine-tagged N, M, E or S protein (mOrVV-NHis, -MHis, -EHis, and -SHis) was generated as previously described, and used as a positive control for each protein. We also used m8rVV-S (17). As shown in Fig. 1*B*, the expression levels of the N and S proteins in the m8rVV-NMES-infected cells were high and moderate, respectively. In contrast, the expression levels of the M and E proteins in m8rVV-NMES-infected cells were weaker than those in mOrVV-MHis- and mOrVV-EHis-infected cells. The M protein in the m8rVV-NMES-infected cells was 20 kDa, whereas that in the mOrVV-MHis-infected cells was observed as forms of ~20 kDa (nonglycosylated form) and 25 kDa (glycosylated form) (23). Furthermore, we investigated the cellular localizations of these structural proteins by indirect immunofluorescence (Fig. 1*C*). In m8rVV-NMES-infected cells, all of the SARS-CoV proteins were localized in the perinuclear regions. In particular, the localization of the N protein in m8rVV-NMES-infected cells was different from that in mOrVV-NHis-infected cells, in which the N-His protein was found diffusely in the cytoplasm. VLPs are formed by the assembly of structural proteins in the cytoplasm, followed by release into the culture medium. By infecting m8rVV-NMES into RK13 cells, we confirmed

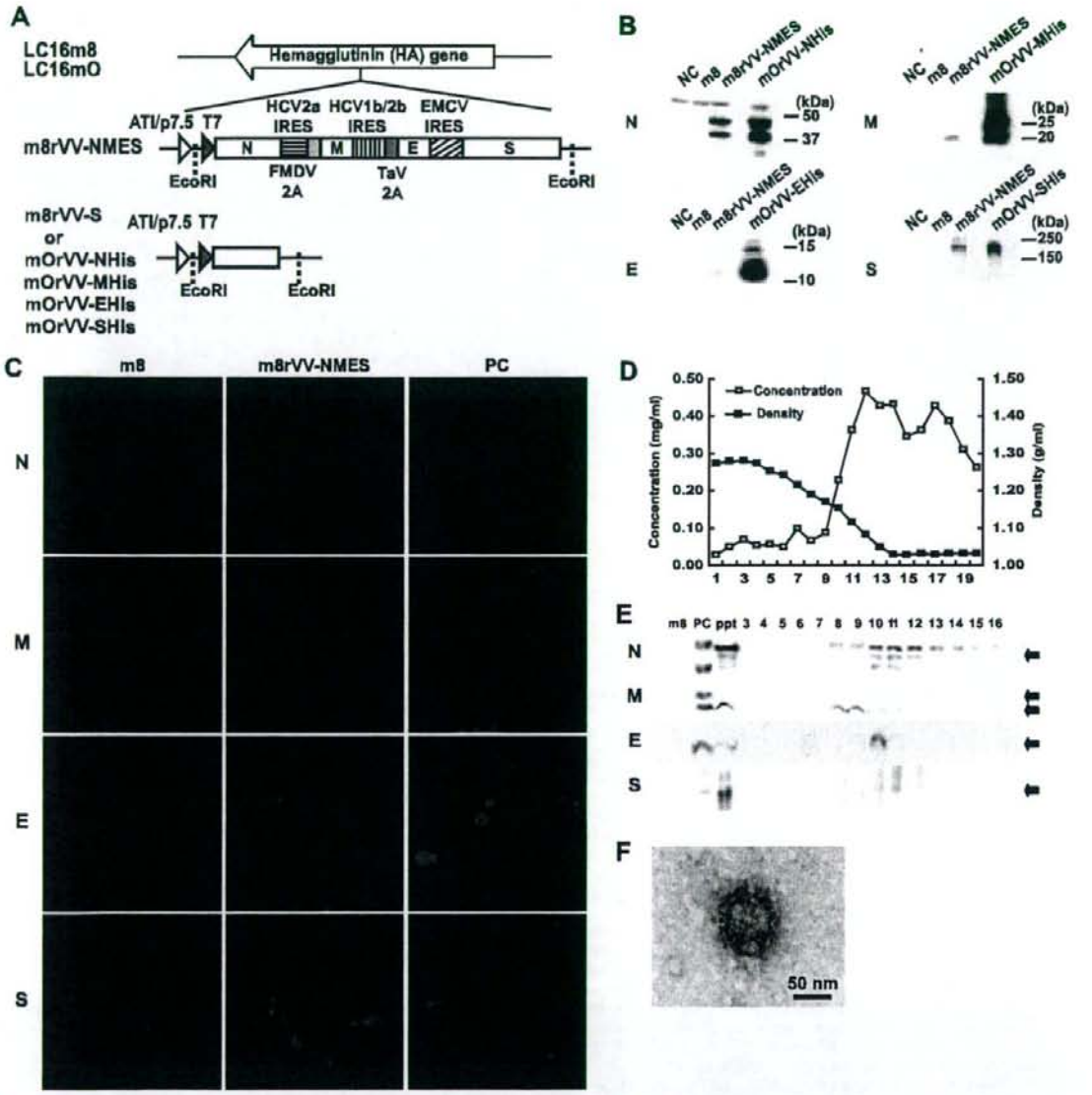

FIGURE 1. Construction of recombinant VV that express four structural proteins of SARS-CoV (m8rVV-NMES). *A*, DNA fragments that encode the SARS-CoV N, M, E, and S proteins were ligated with the internal ribosomal entry site sequence of hepatitis C virus (2a and 1b/2b) and fused with the 2A sequences of foot and mouth disease virus (FMDV) and *Thosea asigna* virus (TaV) or encephalomyocarditis (EMCV). After digestion with *Eco*RI, the DNA fragment was inserted into the pBMSF vector, and the resultant plasmid was designated as pBMSF-NMES. *Pvu*I-linearized pBMSF-NMES was used for homologous recombination into the HA locus of the LC16m8 genome. Recombinant mO that expressed the SARS-CoV N, M, E, or S protein was generated (mOrVV-NHis, -MHis, -EHis, and -SHis) as described in *Materials and Methods*. *B*, Vero E6 cells were infected with m8rVV-NMES or m8. Uninfected Vero E6 cells were used as a negative control (NC). Structural proteins mOrVV-NHis, mOrVV-MHis, mOrVV-EHis, and mOrVV-SHis were used as positive controls. SARS-CoV structural proteins were detected using rabbit polyclonal Abs and donkey anti-rabbit IgG polyclonal Abs, which were conjugated with HRP. The lane between m8rVV-NMES and the mOrVV-N, mOrVV-M, mOrVV-E, and mOrVV-S samples was left empty, to exclude the possibility of leakage of sample solution between lanes. *C*, Vero E6 cells were infected with m8rVV-NMES at an MOI of 5 at 30°C for 4 h. The SARS-CoV proteins in the fixed cells were visualized with the polyclonal Abs against the N, M, or E protein or mAb against the S protein (designated as 13B8). Nuclei were stained with DAPI). Structural proteins mOrVV-NHis, mOrVV-MHis, mOrVV-EHis, and mOrVV-SHis were used as positive controls (PC). *D*, The VLPs were isolated from the culture supernatants of RK13 cells infected with m8rVV-NMES at an MOI of 5 for 48 h at 30°C. After sucrose gradient centrifugation, 20 fractions were collected. *E*, Equal amounts of the gradient fractions (nos. 3–16) were examined by Western blot analyses. m8, m8-infected RK13 cell lysate; ppt, m8rVV-NMES-infected RK13cell lysate; PC, RK13 cell lysates infected with mOrVV-NHis, mOrVV-MHis, mOrVV-EHis, or mOrVV-SHis. *F*, A concentrated culture supernatant was subjected to transmission electron microscopy. VLPs were probed with polyclonal Ab against the S protein and incubated with 5-nm gold-conjugated anti-rabbit IgG.

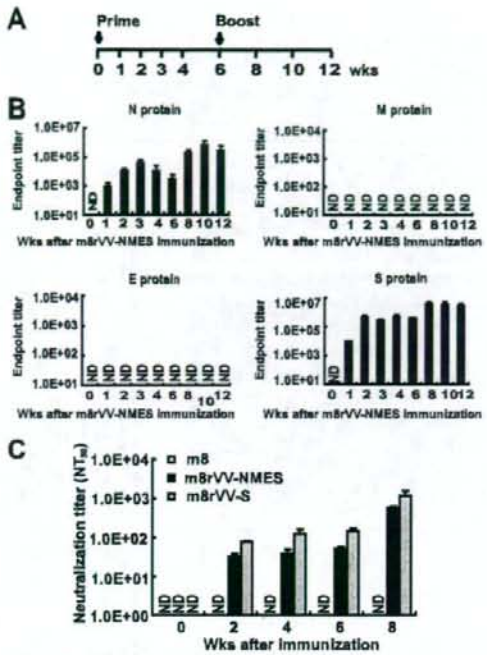

FIGURE 2. Immunogenicity of m8rVV-NMES in rabbits. *A*, New Zealand White rabbits ($n = 3$) were inoculated intradermally with 10^8 PFU/body of m8rVV-NMES or m8 at 0 and 6 wk. Blood samples were collected at the indicated time points. *B*, Induction of serum IgG specific for the four structural proteins of SARS-CoV. The individual SARS-CoV structural protein-specific IgG titers are presented as the end point dilution Ab titers. The end point titer was defined as the reciprocal of the highest dilution of serum at which the absorbance at 490 nm (A_{490}) ratio (A_{490} of m8rVV-NMES-immunized serum/A_{490} of m8-immunized serum (negative control)) was greater than 2.0. *C*, Induction of neutralizing Abs against SARS-CoV. The neutralization titer of m8rVV-NMES-immunized rabbit sera was defined as the end point dilution of the serum at which there was 50% inhibition (NT_{50}) of the SARS-CoV-induced cytopathic effect. Immunization with m8rVVs or m8 was conducted using the schedule described in Fig. 3*A*. ND, Not detectable.

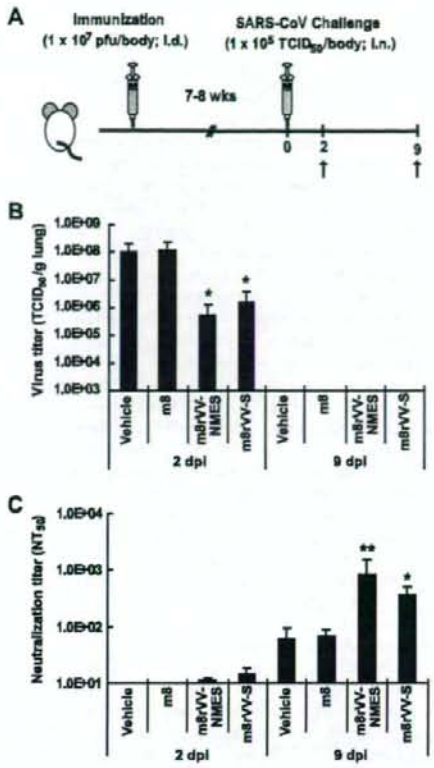

FIGURE 3. SARS-CoV challenge to BALB/c mice immunized with m8rVV-NMES or m8rVV-S. *A*, Four groups of eight BALB/c mice (seven mice in the vehicle-immunized group) were inoculated intradermally with m8rVV-NMES, m8rVV-S, m8, or vehicle and challenged 7–8 wk later with 1×10^5 $TCID_{50}$/body of SARS-CoV delivered via the intranasal route. Blood and lung tissues samples were collected at the indicated time points. *B*, After 2 and 9 days, the titers of SARS-CoV in the lungs of four mice in each group (except for three mice of the vehicle-immunized group, which were examined 2 days later) were determined. Virus titers are expressed as $\log_{10}$ $TCID_{50}$/g of tissue. *C*, At 2 and 9 days after SARS-CoV infection, the serum neutralization titers of all groups were measured as described in *Materials and Methods*. *, $p < 0.05$; **, $p < 0.01$, as compared with both the vehicle- and m8-immunized groups.

the formation of VLPs in the culture medium. After sucrose gradient centrifugation, 20 fractions (500 μl each) were collected (Fig. 1*D*). The four SARS-CoV structural proteins were monitored by Western blot analysis. As shown in Fig. 1*E*, fraction number 10 contained all the SARS-CoV proteins, and the buoyant density of this fraction was ~1.15 g/ml, a value that is consistent with previous reports (18, 24, 25). Moreover, we confirmed the formation of VLPs in the concentrated culture supernatant using scanning electron microscopy and immunogold-labeling with the anti-S protein polyclonal Ab. The particles were 70–100 nm in diameter, which is consistent with the sizes as reported previously (18, 24, 25). The particles were positively stained with immunogold (Fig. 1*F*).

Induction of Abs specific for SARS-CoV structural proteins in rabbits immunized with m8rVV-NMES

To investigate the immunogenicity of m8rVV-NMES, 1×10^8 PFU/body of either m8rVV-NMES or m8, its parental strain, was inoculated intradermally on the backs of New Zealand White rabbits at 0 and 6 wk (Fig. 2*A*). Rabbit antisera specific for the full-length structural proteins of SARS-CoV were detected by ELISA (Fig. 2*B*). In agreement with previous reports (26–28), the N and S proteins both exhibited strong immunogenicity in rabbits. IgG-specific for the N or S protein was induced as early as 1 wk after m8rVV-NMES immunization, and the titer exceeded 1:10000 2 wk later. The titers of Abs against the N and S proteins were dramatically increased by booster immunization with m8rVV-NMES. It was also observed that the Ab titer of the N protein, but not that of the S protein, decreased after reaching the peak titer. Immunization with m8rVV-NMES did not induce Abs specific for the E and M proteins, even after booster immunization (Fig. 2*B*). The antigenicity of the purified E and M proteins coated onto the ELISA plates was confirmed using each rabbit anti-E or anti-M peptide Ab (data not shown). Therefore, we believe that the lack of induction of Abs specific for the E and M proteins in the rabbit sera results from the poor immunogenicity and lower expression levels of these proteins.

Induction of SARS-CoV-neutralizing serum Abs in rabbits by immunizing with m8rVV-NMES

We determined the neutralization titers against SARS-CoV using the same rabbit antisera. The neutralization titer was ~1:30

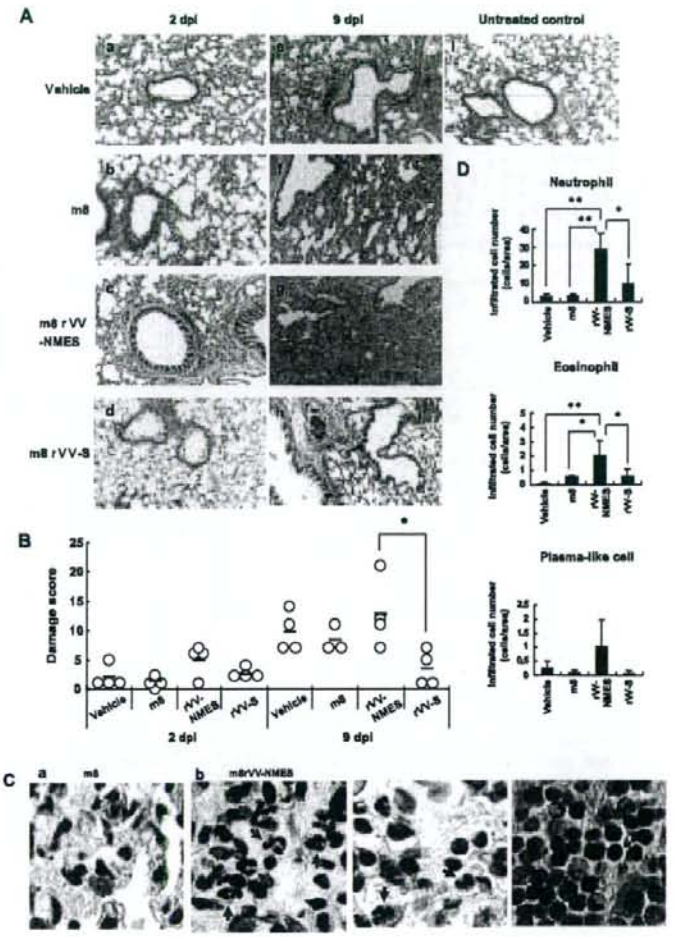

FIGURE 4. Pulmonary histopathology of m8rVV-S-preimmunized BALB/c mice after SARS-CoV challenge. At 7–8 wk after immunization with m8rVV-NMES, m8rVV-S, m8, or vehicle, the mice were infected intranasally with 1×10^5 $TCID_{50}$/body of SARS-CoV. *A*, Four mice from each group (three mice from the vehicle-immunized group were killed 2 days later) were sacrificed 2 and 9 days later. Extirpated lung tissues were fixed with 10% formalin and embedded in paraffin. Paraffin block sections (4-μm thickness) were stained with H&E staining. Histopathologic sections were prepared for vehicle-immunized mice at 2 days postinfection (dpi) (a) and 9 dpi (e), m8-immunized mice at 2 dpi (b) and 9 dpi (f), m8rVV-NMES-immunized mice at 2 dpi (c) and 9 dpi (g), m8rVV-S-immunized mice at 2 dpi (d) and 9 dpi (h), and uninfected mice (i). *B*, The degree of pulmonary inflammation was determined in a blinded fashion on a subjective 27-point scale (0, minimal inflammation; 26, massive inflammation) as described in *Materials and Methods*. Each symbol represents an individual mouse. *, $p < 0.05$. *C*, Representative lung sections from m8-immunized mice (a) and m8rVV-NMES-immunized mice (b) after staining with Luna method (for eosinophils and neutrophils) and H&E (for plasma cells). Arrows indicate neutrophils (yellow), eosinophils (red), and plasma-like cells (green). *D*, The numbers of neutrophils, eosinophils, and plasma-like cells that infiltrated the lung were counted using Luna method and H&E staining. Data are mean ± SD for $n = 5$ mice. Fields viewed at a magnification of ×400. *, $p < 0.05$; **, $p < 0.01$, for significant differences evaluated using the Bonferroni test.

(range, 1:25 to 1:36) after 2 wk, and was sustained for 6 wk (Fig. 2*C*). Booster immunization with m8rVV-NMES further increased the neutralization titer more than 10-fold 2 wk later. These values are somewhat lower than those induced by m8rVV-S in our previous report (17). In contrast, the antisera from rabbits immunized with m8 did not exhibit any neutralizing activity against SARS-CoV (Fig. 2*C*).

SARS-CoV challenge of BALB/c mice having prior immunization with m8rVV-NMES or m8rVV-S

As m8rVV-NMES and m8rVV-S could induce high levels of neutralizing Abs against SARS-CoV (Fig. 2*C*), we investigated the influences of m8rVV-NMES and m8rVV-S on SARS-CoV challenge of BALB/c mice (Fig. 3*A*). The m8rVV-NMES and m8rVV-S constructs were inoculated intradermally on the backs of BALB/c mice at 1×10^7 PFU/body. At 7–8 wk after this single immunization, the mice were infected intranasally with SARS-CoV at 1×10^5 $TCID_{50}$/body. After 2 and 9 days, the lung, liver, small intestine, and spleen were extirpated from the mice under anesthesia, and the SARS-CoV titers were measured. As shown in Fig. 3*B*, 200- and 100-fold reductions in pulmonary virus titers were observed in the m8rVV-NMES-immunized and m8rVV-S-immunized groups 2 days after infection. The virus titers in the lungs of the m8rVV-NMES-immunized and m8rVV-S-immunized groups were 5.40×10^5 and 1.52×10^6 $TCID_{50}$/g of lung, respectively. In contrast, the vehicle-immunized and LC16m8-immunized groups exhibited virus titers of 1.07×10^8 and 1.18×10^8 $TCID_{50}$/g of lung, respectively. The virus was not detected in the lungs of any group 9 days later, as reported previously (11, 15). In contrast, virus titers in other organs, including liver, small intestine, and spleen, were lower than that of the detection limit 2 and 9 days after infection (data not shown).

We also measured the neutralization titers in these mice sera 2 and 9 days after SARS-CoV infection (Fig. 3*C*). Two days postinfection, the neutralization titers of the m8rVV-NMES-immunized and m8rVV-S-immunized groups were 1:11.1 ± 1.01 and 1:14 ± 3.94, respectively, whereas those of the negative control groups were below the limit of detection. At 9 days postinfection, the serum neutralization titers of m8rVV-NMES-immunized and m8rVV-S-immunized groups had increased to 1:838.0 ± 681.0 and 1:367.9 ± 132.1, respectively. In contrast, the serum neutralizing titers of the vehicle-immunized and m8-immunized groups were 1:59.7 ± 35.4 and 1:67.8 ± 18.6, respectively. These results suggest that both the m8rVV-NMES- and m8rVV-S-immunized groups could elicit neutralizing Abs against SARS-CoV and alleviate SARS-CoV infection.

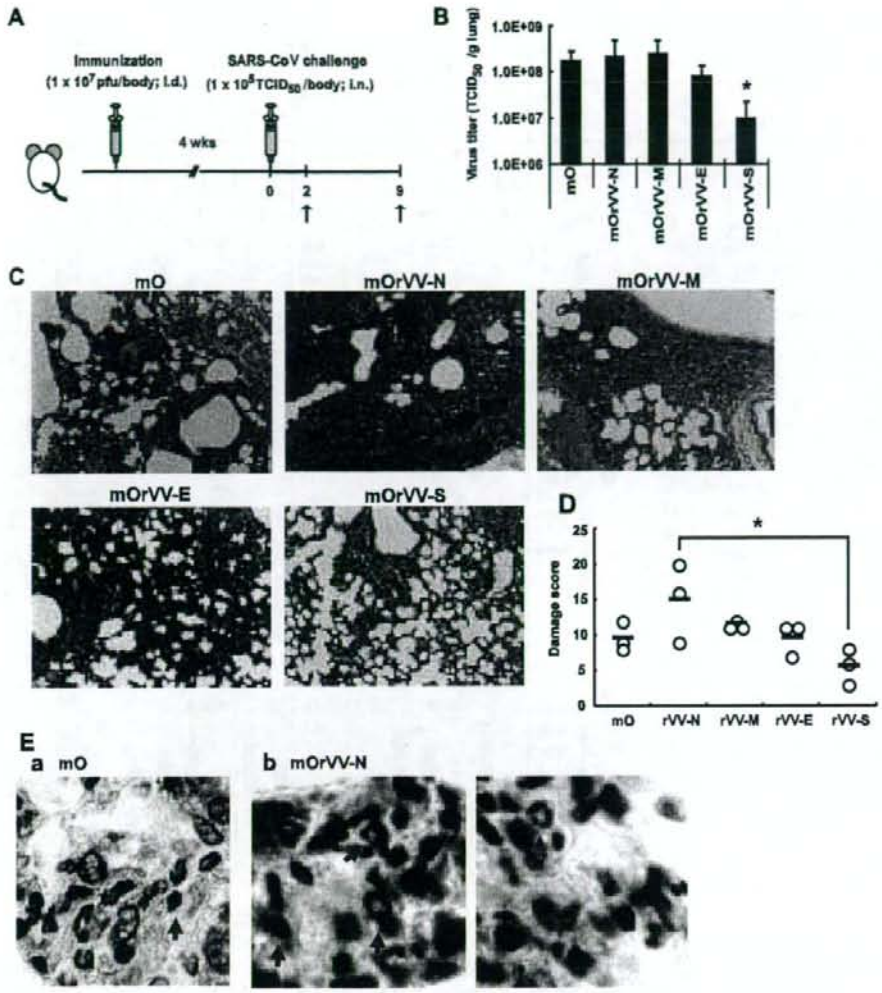

FIGURE 5. Identification of SARS-CoV structural protein implicated in severe pulmonary inflammation. *A*, Five groups of six BALB/c mice were inoculated intradermally with mOrVV-NHis, mOrVV-MHis, mOrVV-EHis, mOrVV-SHis, or mO and challenged 4 wk later with 1×10^5 $TCID_{50}$/body of SARS-CoV via the intranasal route. *B*, After 2 days, the titers of SARS-CoV in the lungs of three mice in each group were determined. Virus titers are expressed as $\log_{10}$ $TCID_{50}$/g of tissue. *, $p < 0.05$, as compared with the mO-immunized group using the Dunnett test. *C*, Histopathologic findings for all the groups 9 days after SARS-CoV infection. Extirpated lung tissues were fixed with 10% formalin and embedded in paraffin. Paraffin block sections (4-μm thickness) were subjected to H&E staining. *D*, The degree of pulmonary inflammation was determined in a blinded fashion on a subjective 27-point scale (0, minimal inflammation; 26, massive inflammation). Each symbol represents an individual mouse. *, $p < 0.05$. *E*, Representative lung sections from mO-immunized mice (a) and mOrVV-N-immunized mice (b) after staining with Luna method (for eosinophils and neutrophils). Arrows indicate neutrophils (yellow) and eosinophils (red).

Histopathologic findings in the lungs of m8rVVs-immunized BALB/c mice after SARS-CoV infection

We performed histopathologic analyses of lung tissues. Two days after SARS-CoV infection, the vehicle-, m8-, and m8rVV-S-immunized groups showed only slight pulmonary inflammation (Fig. 4*A*, a, b, and d), whereas the m8rVV-NMES-immunized group showed infiltration of lymphocytes into the areas surrounding the bronchi and slight thickening of the alveolar epithelium (Fig. 4*A*, c). We scored pulmonary inflammation in all the groups 2 days after SARS-CoV infection as follows (Fig. 4*B*): in the m8rVV-NMES-immunized group, 5.00 ± 2.71; in the vehicle-immunized group, 2.00 ± 2.00; in the m8-immunized group, 1.33 ± 0.82; and in the m8rVV-S-immunized group, 2.50 ± 1.00. At 9 days postinfection, the vehicle-, m8-, and m8rVV-NMES-immunized groups exhibited severe pulmonary inflammation, i.e., infiltration of inflammatory cells and thickening of alveolar epithelia (Fig. 4*A*, e, f, and g). In contrast, the m8rVV-S-immunized group showed only slight pulmonary inflammation (Fig. 4*A*, h). As shown in Fig. 4*B*, the pulmonary inflammation score for the m8rVV-NMES-immunized group (12.75 ± 2.87) 9 days after SARS-CoV infection was significantly higher than that for the m8rVV-S-immunized group (3.50 ± 3.00). In contrast, this score was comparable to those obtained for the vehicle-immunized and m8-immunized groups (9.75 ± 2.87 and

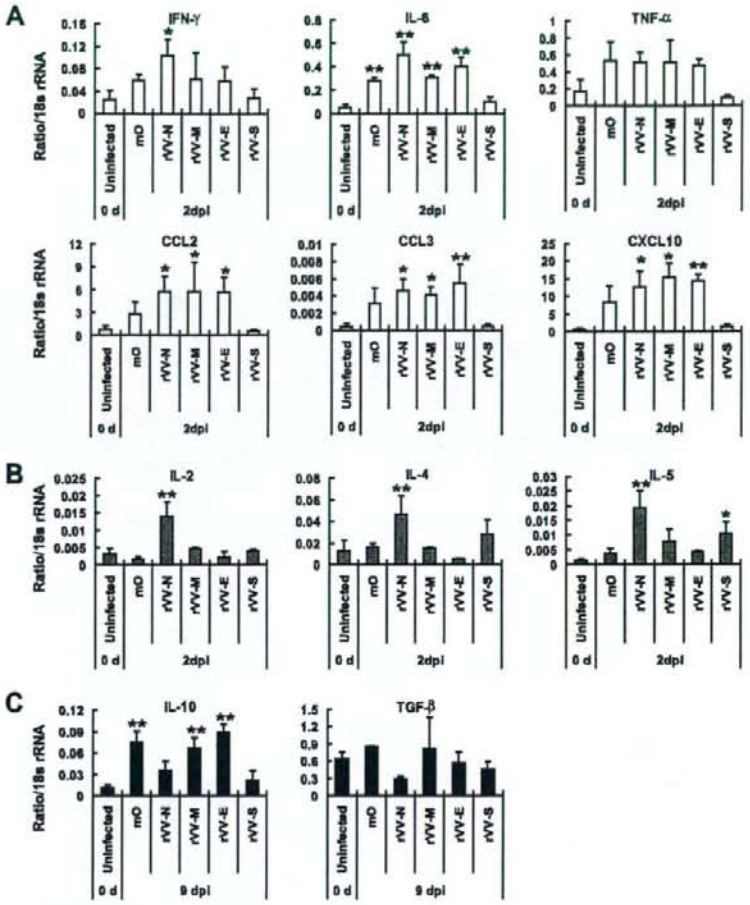

FIGURE 6. Cytokine profiles of the lungs of BALB/c mice preimmunized with each SARS-CoV structural protein and challenged with SARS-CoV. Three mice from each group were sacrificed 2 and 9 days postinfection. The total RNA of the lung was extracted. Quantitative RT-PCR was conducted as described in *Materials and Methods*. The fold change in copy number of each cytokine or chemokine mRNA was calculated by the $2^{-\Delta\Delta Ct}$ method using 18 S rRNA as an endogenous calibrator. *, $p < 0.05$; **, $p < 0.01$, as compared with the uninfected control group using the Bonferroni test. *A*, The levels of mRNA for proinflammatory cytokines and chemokines 2 days after SARS-CoV infection. *B*, The mRNA expression levels of cytokines related to T cell activation 2 days after SARS-CoV infection. *C*, The mRNA expression levels of anti-inflammatory cytokines 9 days after SARS-CoV infection.

8.33 ± 2.31, respectively). The m8rVV-NMES-immunized group exhibited as severe inflammation as the control groups, although m8rVV-NMES contains the S protein and protects as well as m8rVV-S against SARS-CoV infection. In addition, marked infiltration of neutrophils, eosinophils, plasma-like cells, and lymphocytes was observed in the m8rVV-NMES-immunized group, as compared with the control groups, after SARS-CoV infection (Fig. 4*C*, b and *D*).

These results suggest that the severe pulmonary inflammation seen in m8rVV-NMES-immunized mice after SARS-CoV infection results from host immune responses rather than a direct cytopathic effect of SARS-CoV, because the virus titers for all the group were negligible 9 days after SARS-CoV infection and the virus titer of the m8rVV-NMES-immunized group was significantly decreased 2 days postinfection.

Identification of the factor that results in the exacerbation of pulmonary inflammation in m8rVV-NMES-immunized BALB/c mice after SARS-CoV infection

We hypothesized that the severe pulmonary inflammation seen in the m8rVV-NMES-immunized mice resulted from the host immune responses to SARS-CoV components expressed by m8rVV-NMES. This notion was supported by the observation of negligible virus titers 9 days after SARS-CoV infection. Therefore, we investigated the influence of recombinant VV expressing each structural protein of SARS-CoV (mOrVV-NHis, mOrVV-MHis, mOrVV-EHis, and mOrVV-SHis) on subsequent intranasal infection with SARS-CoV. BALB/c mice were immunized with mOrVV-NHis, -MHis, -EHis, and -SHis at 1×10^7 PFU/body, and 4 wk later infected intradermally with 1×10^5 $TCID_{50}$ of SARS-CoV (Fig. 5*A*). After 2 and 9 days, three mice from each group were sacrificed following blood collection under anesthesia, and their lungs were extirpated. Consistent with earlier results, a significant reduction of pulmonary virus titer was observed after 2 days in only the mOrVV-SHis-immunized group (Fig. 5*B*). In contrast, immunization with the other SARS-CoV structural proteins, including the N, M, and E proteins, did not confer protection against the subsequent SARS-CoV infection. As shown in Fig. 5*C*, the alleviation of pulmonary inflammation was also observed in the mOrVV-SHis-immunized group. Severe infiltration of lymphocytes and thickening of the alveolar epithelia were observed in the lung tissues of the mOrVV-NHis-immunized mice 9 days after SARS-CoV infection (Fig. 5*C*). The pulmonary damage in the mOrVV-NHis-immunized mice (15.00 ± 5.56) was significantly more severe than that in the mOrVV-SHis-immunized mice (5.67 ± 2.52) (Fig. 5*D*). However, there were no significant differences among the other groups. Furthermore, infiltration of neutrophils, eosinophils, and lymphocytes was observed in the

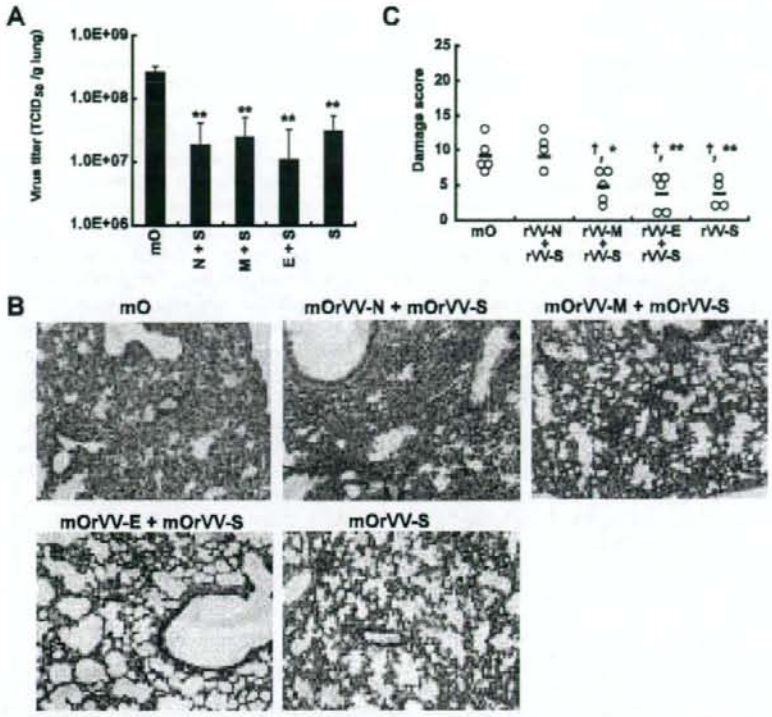

FIGURE 7. Severe pneumonia in BALB/c mice that were previously immunized with the combination of N protein and S protein of SARS-CoV. *A*, Five groups of BALB/c mice (n = 8–10 per group) were inoculated intradermally with the combinations of mOrVV-NHis and mOrVV-SHis (mOrVV-N + S), mOrVV-MHis and mOrVV-SHis (mOrVV-M + S), mOrVV-EHis and mOrVV-SHis (mOrVV-E + S), mOrVV-SHis, and mO, and challenged 7 wk later with 1×10^5 $TCID_{50}$/body of SARS-CoV via the intranasal route. After 2 days, the titers of SARS-CoV in the lungs of n = 3–5 mice from each group were determined. Virus titers are expressed as $\log_{10}$ $TCID_{50}$/g of tissue. *, $p < 0.05$, **, $p < 0.01$, as compared with the mO-immunized group using the Bonferroni test. *B*, Histopathologic findings for all the groups 9 days after SARS-CoV infection. Extirpated lung tissues were fixed with 10% formalin and embedded in paraffin. Paraffin block sections (4-μm thickness) were subjected to H&E staining. *C*, The degree of pulmonary inflammation was determined in a blinded fashion on a subjective 27-point scale (0, minimal inflammation; 26, massive inflammation). Each symbol represents an individual mouse. †, $p < 0.05$; ‡, $p < 0.01$, as compared with the mO-immunized group using the Bonferroni test. *, $p < 0.05$; **, $p < 0.01$, as compared with the mOrVV-N + S-immunized group using the Bonferroni test.

mOrVV-NHis-immunized mice after SARS-CoV infection (Fig. 5*E*, b), although the extent of infiltration of these cells into the lungs of these mice was somewhat lower than that observed in the m8rVV-NMES-immunized mice after SARS-CoV infection (Fig. 4*D*). This may explain the observed differences in the histopathologic findings for the mOrVV-NHis-immunized mice and m8rVV-NMES-immunized mice.

Pulmonary cytokine responses of SARS-CoV-infected BALB/c mice previously immunized with recombinant VV expressing each structural protein of SARS-CoV

To elucidate the reason for the severe pulmonary inflammation observed in the mOrVV-NHis-immunized mice after SARS-CoV infection, we measured by quantitative RT-PCR the mRNA levels for various cytokines and chemokines in the lungs of BALB/c mice preimmunized with mOrVV-NHis, -MHis, -EHis, -SHis, or mO. Several proinflammatory cytokine and chemokine mRNAs, including those for IL-6, CXCL10, CCL2, and CCL3, were increased in all the groups, with the exception of the mOrVV-SHis group, 2 days after SARS-CoV infection (Fig. 6*A*). In contrast, the mOrVV-SHis-immunized group showed low levels of mRNA expression for these proinflammatory cytokines or chemokines, especially IL-6, resulting in reduced lung pathology after immunization. The mRNA levels for IFN-γ, IL-2, IL-4, and IL-5 were highest in the mOrVV-NHis-immunized group (Fig. 6, *A* and *B*). None of the other groups showed up-regulation of these cytokines, with the exception of the IL-5 mRNA level in the mOrVV-SHis-immunized group. Furthermore, the mRNA expression levels of anti-inflammatory cytokines (IL-10 and TGF-β) in the mOrVV-NHis-immunized group were markedly lower than expression levels in any of the other groups, which exhibited high virus titers, and were comparable to those of the mOrVV-SHis group, in which pulmonary inflammation was alleviated (Fig. 6*C*).

Verification of exacerbating effect of prior immunization with N protein in SARS-CoV-infected Balb/c mice

To verify the exacerbating effect of N protein immunization, we investigated the pulmonary virus titers and histopathology in BALB/c mice that were previously immunized with the combination of mOrVV-N and mOrVV-S (mOrVV-N+S-immunized group) 2 and 9 days after SARS-CoV infection, and compared them to those of all other groups, including the mO-, mOrVV-M+S-, mOrVV-E+S-, and mOrVV-S-immunized groups. The mOrVV-N+S-immunized group showed significantly decreased pulmonary virus titers compared with the mO-immunized group (Fig. 7*A*). However, the mOrVV-N+S-immunized group exhibited as

severe pneumonia as the mO-immunized group (Fig. 7, *B* and *C*). In contrast, both the mOrVV-M+S-immunized group and the mOrVV-E+S-immunized group were protected against SARS-CoV infection to the same extent as the mOrVV-S-immunized group (Fig. 7, *A–C*).

Discussion

SARS-CoV is newly identified as an agent of SARS. However, the detailed mechanism by which SARS-CoV causes severe pneumonia remains unclear. The uncontrolled release of immune mediators has been implicated in the pathogenesis of SARS, whereas the cytokine profiles of SARS patients have not elucidated the cause the pneumonia owing to their diversity. It seems likely that the diverse cytokine profiles noted among adult SARS patients are related to patient anamnesis.

In the present study, we observed severe pulmonary inflammation in m8rVV-NMES-immunized BALB/c mice 9 days after SARS-CoV infection (Fig. 4*A*, g), even though the initial virus titer was significantly lower than those of the control groups, which included vehicle- and m8-immunized mice (Fig. 3*B*). The severity of pulmonary inflammation did not correlate with the virus titer in the m8rVV-NMES-immunized mice, in contrast to the correlations observed for the vehicle-, m8-, and m8rVV-S-immunized groups. We identified the N protein of SARS-CoV as the cause of the severe pneumonia observed during SARS-CoV infection (Fig. 5, *C* and *D*, and 7, *B* and *C*). To date, no studies have been reported to our knowledge regarding SARS patients with severe pneumonia who were previously immunized with either SARS-CoV or a highly related species. In contrast, there are several reports of antisera against human CoV (229E and OC43) and host factor IL-11 cross-reacting with the SARS-CoV Ag (29, 30). Furthermore, the N protein of SARS-CoV has been shown to induce both cellular and humoral immune responses (31–33). Taken together, these results raise the possibility that a percentage of SARS patients already possess the adaptive immune response elements that can interact with SARS-CoV components, including the N protein, and that their adaptive immune response may be involved in the exacerbation of pneumonia. The temporal changes in immune response and the pathogenesis after SARS-CoV infection of an animal model that had previously been immunized with SARS-CoV components are not well understood, as almost all the previous studies reported only protection within a few days of SARS-CoV infection (34–39). In the present study, we demonstrate that mOrVV-NHis-immunized mice after SARS-CoV infection exhibit an imbalance between T cell activation (high expression levels of IFN-γ, IL-2, IL-4, and IL-5) and subsequent suppression (low expression levels of IL-10 and TGF-β), as well as high-level production of proinflammatory cytokines (IL-6 and TNF-α) and chemokines (CCL2, CCL3, and CXCL10). Jiang et al. (40) reported elevation of CXCL10 or IP-10 production in the pneumocytes, $CD3^+$ T cells, and monocytes and macrophages of the lungs of patients with SARS. CXCL10 may be responsible for the infiltration of activated T cells and monocytes or macrophages, which is a pathologic finding in SARS patients (41–43). It has been reported that elevated expression of monocyte or macrophage activation factors (CCL2 and CCL3) was observed in SARS patients (8, 44). Furthermore, the highest expression of IL-6 in mOrVV-NHis-immunized mice is reasonable (Fig. 6*A*), as the elevation of IL-6 levels is considered one of the causes in the severe pneumonia of SARS patients. Zhang et al. (45) reported recently the molecular mechanism of IL-6 expression induction by the N protein of SARS-CoV. In contrast, both IL-10 and TGF-β play important roles in suppressing inflammatory responses (46). Thus, the reduced production of both anti-inflammatory cytokines in the mOrVV-NHis-immunized mice after SARS-CoV infection may be related to the severity of the pulmonary inflammation in these mice. Weingartl et al. (47) and Czub et al. (48) reported that immunization with S protein expressing-recombinant modified VV Ankara (rMVA-S) induced stronger inflammatory responses and focal necrosis in liver tissues after SARS-CoV challenge than in control animals. However, the precise mechanism underlying this liver inflammation has not been clarified. Feline infectious peritonitis virus, which is another member of the coronavirus family, exhibits enhanced infection into monocytes or macrophages through virus-specific Ab binding to the Fc receptors of these cells and causes enhanced inflammation (49). It has also been reported for dengue virus that secondary infection with a different genotype results in more severe symptoms, including dengue hemorrhagic fever and dengue shock syndrome. The exacerbation of this symptom is also positively associated with pre-existing Abs with specificity for dengue virus (50). In the case of SARS-CoV, Ab-dependent enhancement of infection has not been reported previously. We hypothesized that the severe pneumonia observed in mOrVV-NHis-immunized mice after SARS-CoV infection does not result from Ab-dependent enhancement because the virus titers in the mouse lungs 9 days later were below the detection limit. Deming et al. (51) reported recently the intensive infiltration of eosinophils as well as lymphocytes after SARS-CoV infection of aged BALB/c mice previously immunized with the N protein of SARS-CoV. It has also been reported that immunization with formalin-inactivated respiratory syncytial virus vaccine and VV that expresses the G glycoprotein of respiratory syncytial virus correlates with the augmentation of Th2-type immune responses and enhanced pulmonary disease (52, 53). Therefore, the authors speculated that the Th2-biased responses of vaccinated hosts after SARS-CoV infection might aggravate pulmonary inflammation, although the main host response remains unknown. In contrast, our current data suggest that N protein-immunized mice exhibit activation of both Th1 and Th2 responses after SARS-CoV infection. In agreement with our data, Jin et al. (54) have demonstrated that prior immunization with N protein generates stronger Ag-specific Th1 and Th2 responses than immunization with M or E protein. In addition, we demonstrate the suppression of anti-inflammatory cytokine responses in N protein-immunized mice. Interestingly, Shi et al. (55) demonstrated that coinjection of M protein with N protein not only enhanced the production of Th1 cytokines (IFN-γ and IL-2), but also reduced the rates of mortality and pathologic change in SARS-CoV-infected voles. These results suggest that further studies, including epitope analysis, are required to reveal the precise mechanism underlying the severe pulmonary inflammation that results from SARS-CoV infection of BALB/c mice immunized with the N protein of SARS-CoV.

In contrast, intradermal immunization of aged BALB/c mice with m8rVV-S at 1×10^7 PFU/body significantly reduced the pulmonary virus titer 2 days after SARS-CoV infection (Fig. 3*B*). Furthermore, the m8rVV-S-immunized group exhibited alleviation of the pulmonary histopathology, as compared with both control groups after 9 days. To date, various types of SARS vaccine, including recombinant vaccines, inactivated vaccines, and DNA vaccine, have been reported (34–39). There are only a few reports on the effect of a single immunization with recombinant SARS vaccines, namely SARS-CoV S protein-expressing vaccines based on rabies virus (56), vesicular stomatitis virus (39), and adeno-associated virus (57). It is noteworthy that a single i.m. immunization with recombinant adeno-associated virus that expresses the receptor-binding domain of S protein conferred long-term protection against SARS-CoV infection (57). In the present study, we also show that a single immunization with m8rVV-S reduces viral load and improves the histopathologic findings in the lungs of BALB/c

mice infected with high-titer (1×10^5 $TCID_{50}$/body) SARS-CoV, although a relatively low titer of SARS-CoV was used in the previous study conducted by Du et al. (57). These results suggest that the systemic immune responses induced by a single immunization with SARS vaccine successfully protect the animal model against intranasal SARS-CoV infection.

In summary, we demonstrate that the immunization of BALB/c mice with the N protein of SARS-CoV causes severe pulmonary inflammation upon subsequent SARS-CoV infection, probably via the imbalance created between T cell activation and suppression, as well as by massive proinflammatory cytokine production. These results provide new insights into the mechanisms involved in the pathogenesis of SARS and help in the development of safe vaccines.

Acknowledgments

We are grateful to Dr. Ryuichi Miura (University of Tokyo) for arranging the SARS-CoV challenge experiment. We are also grateful to Iyo Kataoka (Institute of Medical Science, University of Tokyo). We thank Dr. Masahiro Shuda of the University of Pittsburgh for helpful discussions. We also thank Dr. Tetsuya Mizutani and Dr. Shigeru Morikawa (Department of Virology I, National Institute of Infectious Diseases) for providing antisera from rabbits immunized with the M protein peptide and inactivated SARS-CoV particles.

Disclosures

The authors have no financial conflict of interest.

References

1. Drosten, C., S. Gunther, W. Preiser, S. van der Werf, H. R. Brodt, S. Becker, H. Rabenau, M. Panning, L. Kolesnikova, R. A. Fouchier, et al. 2003. Identification of a novel coronavirus in patients with severe acute respiratory syndrome. *N. Engl. J. Med.* 348: 1967–1976.
2. Ksiazek, T. G., D. Erdman, C. S. Goldsmith, S. R. Zaki, T. Peret, S. Emery, S. Tong, C. Urbani, J. A. Comer, W. Lim, et al. 2003. A novel coronavirus associated with severe acute respiratory syndrome. *N. Engl. J. Med.* 1953–1966.
3. Peiris, J. S., S. T. Lai, L. L. Poon, Y. Guan, L. Y. Yam, W. Lim, J. Nicholls, W. K. Yee, W. W. Yan, M. T. Cheung, et al. 2003. Coronavirus as a possible cause of severe acute respiratory syndrome. *Lancet* 361: 1319–1325.
4. Rota, P. A., M. S. Oberste, S. S. Monroe, W. A. Nix, R. Campagnoli, J. P. Icenogle, S. Penaranda, B. Bankamp, K. Maher, M. H. Chen, et al. 2003. Characterization of a novel coronavirus associated with severe acute respiratory syndrome. *Science* 300: 1394–1399.
5. Li, W., M. J. Moore, N. Vasilieva, J. Sui, S. K. Wong, M. A. Berne, M. Somasundaran, J. L. Sullivan, K. Luzuriaga, T. C. Greenough, et al. 2003. Angiotensin-converting enzyme 2 is a functional receptor for the SARS coronavirus. *Nature* 426: 450–454.
6. Hamming, I., W. Timens, M. L. Bulthuis, A. T. Lely, G. J. Navis, and H. van Goor. 2004. Tissue distribution of ACE2 protein, the functional receptor for SARS coronavirus. A first step in understanding SARS pathogenesis. *J. Pathol.* 203: 631–637.
7. Jones, B. M., E. S. Ma, J. S. Peiris, P. C. Wong, J. C. Ho, B. Lam, K. N. Lai, and K. W. Tsang. 2004. Prolonged disturbances of in vitro cytokine production in patients with severe acute respiratory syndrome (SARS) treated with ribavirin and steroids. *Clin. Exp. Immunol.* 135: 467–473.
8. Wong, C. K., C. W. Lam, A. K. Wu, W. K. Ip, N. L. Lee, I. H. Chan, L. C. Lit, D. S. Hui, M. H. Chan, S. S. Chung, and J. J. Sung. 2004. Plasma inflammatory cytokines and chemokines in severe acute respiratory syndrome. *Clin. Exp. Immunol.* 136: 95–103.
9. Rowe, T., G. Gao, R. J. Hogan, R. G. Crystal, T. G. Voss, R. L. Grant, P. Bell, G. P. Kobinger, N. A. Wivel, and J. M. Wilson. 2004. Macaque model for severe acute respiratory syndrome. *J. Virol.* 78: 11401–11404.
10. Osterhaus, A. D., R. A. Fouchier, and T. Kuiken. 2004. The aetiology of SARS: Koch's postulates fulfilled. *Philos. Trans. R. Soc. Lond B Biol. Sci.* 359: 1081–1082.
11. Subbarao, K., J. McAuliffe, L. Vogel, G. Fahle, S. Fischer, K. Tatti, M. Packard, W. J. Shieh, S. Zaki, and B. Murphy. 2004. Prior infection and passive transfer of neutralizing antibody prevent replication of severe acute respiratory syndrome coronavirus in the respiratory tract of mice. *J. Virol.* 78: 3572–3577.
12. Glass, W. G., K. Subbarao, B. Murphy, and P. M. Murphy. 2004. Mechanisms of host defense following severe acute respiratory syndrome-coronavirus (SARS-CoV) pulmonary infection of mice. *J. Immunol.* 173: 4030–4039.
13. Roberts, A., L. Vogel, J. Guarner, N. Hayes, B. Murphy, S. Zaki, and K. Subbarao. 2005. Severe acute respiratory syndrome coronavirus infection of golden Syrian hamsters. *J. Virol.* 79: 503–511.
14. ter Meulen, J., A. B. Bakker, E. N. van den Brink, G. J. Weverling, B. E. Martina, B. L. Haagmans, T. Kuiken, J. de Kruif, W. Preiser, W. Spaan, et al. 2004. Human monoclonal antibody as prophylaxis for SARS coronavirus infection in ferrets. *Lancet* 363: 2139–2141.
15. Roberts, A., C. Paddock, L. Vogel, E. Butler, S. Zaki, and K. Subbarao. 2005. Aged BALB/c mice as a model for increased severity of severe acute respiratory syndrome in elderly humans. *J. Virol.* 79: 5833–5838.
16. Hong, T. C., Q. L. Mai, D. V. Cuong, M. Parida, H. Minekawa, T. Notomi, F. Hasebe, and K. Morita. 2004. Development and evaluation of a novel loop-mediated isothermal amplification method for rapid detection of severe acute respiratory syndrome coronavirus. *J. Clin. Microbiol.* 42: 1956–1961.
17. Kitabatake, M., S. Inoue, F. Yasui, S. Yokochi, M. Arai, K. Morita, H. Shida, M. Kidokoro, F. Murai, M. Q. Le, K. Mizuno, et al. 2007. SARS-CoV spike protein-expressing recombinant vaccinia virus efficiently induces neutralizing antibodies in rabbits pre-immunized with vaccinia virus. *Vaccine* 25: 630–637.
18. Hsieh, P. K., S. C. Chang, C. C. Huang, T. T. Lee, C. W. Hsiao, Y. H. Kou, I. Y. Chen, C. K. Chang, T. H. Huang, and M. F. Chang. 2005. Assembly of severe acute respiratory syndrome coronavirus RNA packaging signal into virus-like particles is nucleocapsid dependent. *J. Virol.* 79: 13848–13855.
19. Zhang, C. H., J. H. Lu, Y. F. Wang, H. Y. Zheng, S. Xiong, M. Y. Zhang, X. J. Liu, J. X. Li, Z. Y. Wan, X. G. Yan, et al. 2005. Immune responses in BALB/c mice induced by a candidate SARS-CoV inactivated vaccine prepared from F69 strain. *Vaccine* 23: 3196–3201.
20. Biacchesi, S., M. H. Skiadopoulos, L. Yang, B. R. Murphy, P. L. Collins, and U. J. Buchholz. 2005. Rapid human metapneumovirus microneutralization assay based on green fluorescent protein expression. *J. Virol. Methods* 128: 192–197.
21. Cimolai, N., G. P. Taylor, D. Mah, and B. J. Morrison. 1992. Definition and application of a histopathological scoring scheme for an animal model of acute *Mycoplasma pneumoniae* pulmonary infection. *Microbiol. Immunol.* 36: 465–478.
22. Luna, L. G., 1968. *Manual of Histologic Staining Methods of the Armed Forces Institute of Pathology.* McGraw-Hill, New York, p. 111.
23. Voss, D., A. Kern, E. Traggiai, M. Eickmann, K. Stadler, A. Lanzavecchia, and S. Becker. 2006. Characterization of severe acute respiratory syndrome coronavirus membrane protein. *FEBS Lett.* 580: 968–973.
24. Ho, Y., P. H. Lin, C. Y. Liu, S. P. Lee, and Y. C. Chao. 2004. Assembly of human severe acute respiratory syndrome coronavirus-like particles. *Biochem. Biophys. Res. Commun.* 318: 833–838.
25. Huang, Y., Z. Y. Yang, W. P. Kong, and G. J. Nabel. 2004. Generation of synthetic severe acute respiratory syndrome coronavirus pseudoparticles: implications for assembly and vaccine production. *J. Virol.* 78: 12557–12565.
26. Buchholz, U. J., A. Bukreyev, L. Yang, E. W. Lamirande, B. R. Murphy, K. Subbarao, and P. L. Collins. 2004. Contributions of the structural proteins of severe acute respiratory syndrome coronavirus to protective immunity. *Proc. Natl. Acad. Sci. USA* 101: 9804–9809.
27. Kim, T. W., J. H. Lee, C. F. Hung, S. Peng, R. Roden, M. C. Wang, R. Viscidi, Y. C. Tsai, L. He, P. J. Chen, et al. 2004. Generation and characterization of DNA vaccines targeting the nucleocapsid protein of severe acute respiratory syndrome coronavirus. *J. Virol.* 78: 4638–4645.
28. Fan, B. X., L. X. Xie, L. A. Chen, W. J. Chen, J. Wen, and Y. N. Liu. 2005. Study on the dynamics of IgG antibody in 311 patients with severe acute respiratory syndrome. *Zhonghua Liu Xing Bing Xue Za Zhi.* 26: 194–196.
29. Che, X. Y., L. W. Qiu, Z. Y. Liao, Y. D. Wang, K. Wen, Y. X. Pan, W. Hao, Y. B. Mei, V. C. Cheng, and K. Y. Yuen. 2005. Antigenic cross-reactivity between severe acute respiratory syndrome-associated coronavirus and human coronaviruses 229E and OC43. *J. Infect. Dis.* 191: 2033–2037.
30. Cheng, M., C. W. Chan, R. C. Cheung, R. K. Bikkavilli, Q. Zhao, S. W. Au, P. K. Chan, S. S. Lee, G. Cheng, W. K. Ho, and W. T. Cheung. 2005. Cross-reactivity of antibody against SARS-coronavirus nucleocapsid protein with IL-11. *Biochem. Biophys. Res. Commun.* 338: 1654–1660.
31. Liu, S. J., C. H. Leng, S. P. Lien, H. Y. Chi, C. Y. Huang, C. L. Lin, W. C. Lian, C. J. Chen, S. L. Hsieh, and P. Chong. 2006. Immunological characterizations of the nucleocapsid protein based SARS vaccine candidates. *Vaccine* 24: 3100–3108.
32. Zhu, M. S., Y. Pan, H. Q. Chen, Y. Shen, X. C. Wang, Y. J. Sun, and K. H. Tao. 2004. Induction of SARS-nucleoprotein-specific immune response by use of DNA vaccine. *Immunol. Lett.* 92: 237–243.
33. Zhao, J., Q. Huang, W. Wang, Y. Zhang, P. Lv, and X. M. Gao. 2007. Identification and characterization of dominant helper T-cell epitopes in the nucleocapsid protein of severe acute respiratory syndrome coronavirus. *J. Virol.* 81: 6079–6088.
34. Yang, Z. Y., W. P. Kong, Y. Huang, A. Roberts, B. R. Murphy, K. Subbarao, and G. J. Nabel. 2004. A DNA vaccine induces SARS coronavirus neutralization and protective immunity in mice. *Nature* 428: 561–564.
35. Bukreyev, A., E. W. Lamirande, U. J. Buchholz, L. N. Vogel, W. R. Elkins, M. St Claire, B. R. Murphy, K. Subbarao, and P. L. Collins. 2004. Mucosal immunisation of African green monkeys (*Cercopithecus aethiops*) with an attenuated parainfluenza virus expressing the SARS coronavirus spike protein for the prevention of SARS. *Lancet* 363: 2122–2127.
36. Zhi, Y., J. Figueredo, G. P. Kobinger, H. Hagan, R. Calcedo, J. R. Miller, G. Gao, and J. M. Wilson. 2006. Efficacy of severe acute respiratory syndrome vaccine based on a nonhuman primate adenovirus in the presence of immunity against human adenovirus. *Hum. Gene Ther.* 17: 500–506.
37. Bisht, H., A. Roberts, L. Vogel, K. Subbarao, and B. Moss. 2005. Neutralizing antibody and protective immunity to SARS coronavirus infection of mice induced by a soluble recombinant polypeptide containing an N-terminal segment of the spike glycoprotein. *Virology* 334: 160–165.
38. Bisht, H., A. Roberts, L. Vogel, A. Bukreyev, P. L. Collins, B. R. Murphy, K. Subbarao, and B. Moss. 2004. Severe acute respiratory syndrome coronavirus

spike protein expressed by attenuated vaccinia virus protectively immunizes mice. *Proc. Natl. Acad. Sci. USA* 101: 6641–6646.
39. Kapadia, S. U., J. K. Rose, E. Lamirande, L. Vogel, K. Subbarao, and A. Roberts. 2005. Long-term protection from SARS coronavirus infection conferred by a single immunization with an attenuated VSV-based vaccine. *Virology* 340: 174–182.
40. Jiang, Y., J. Xu, C. Zhou, Z. Wu, S. Zhong, J. Liu, W. Luo, T. Chen, Q. Qin, and P. Deng. 2005. Characterization of cytokine/chemokine profiles of severe acute respiratory syndrome. *Am. J. Respir. Crit. Care Med.* 171: 850–857.
41. Franks, T. J., P. Y. Chong, P. Chui, J. R. Galvin, R. M. Lourens, A. H. Reid, E. Selbs, C. P. McEvoy, C. D. Hayden, J. Fukuoka, et al. 2003. Lung pathology of severe acute respiratory syndrome (SARS): a study of 8 autopsy cases from Singapore. *Hum. Pathol.* 34: 743–748.
42. Nicholls, J. M., L. L. Poon, K. C. Lee, W. F. Ng, S. T. Lai, C. Y. Leung, C. M. Chu, P. K. Hui, K. L. Mak, W. Lim, et al. 2003. Lung pathology of fatal severe acute respiratory syndrome. *Lancet* 361: 1773–1778.
43. Ding, Y., H. Wang, H. Shen, Z. Li, J. Geng, H. Han, J. Cai, X. Li, W. Kang, D. Weng, et al. 2003. The clinical pathology of severe acute respiratory syndrome (SARS): a report from China. *J. Pathol.* 200: 282–289.
44. He, L., Y. Ding, Q. Zhang, X. Che, Y. He, H. Shen, H. Wang, Z. Li, L. Zhao, J. Geng, et al. 2006. Expression of elevated levels of pro-inflammatory cytokines in SARS-CoV-infected ACE2+ cells in SARS patients: relation to the acute lung injury and pathogenesis of SARS. *J. Pathol.* 210: 288–297.
45. Zhang, X., K. Wu, D. Wang, X. Yue, D. Song, Y. Zhu, and J. Wu. 2007. Nucleocapsid protein of SARS-CoV activates interleukin-6 expression through cellular transcription factor NF-κB. *Virology* 365: 324–335.
46. Fuss, I. J., M. Boirivant, B. Lacy, and W. Strober. 2002. The interrelated roles of TGF-β and IL-10 in the regulation of experimental colitis. *J. Immunol.* 168: 900–908.
47. Weingartl, H., M. Czub, S. Czub, J. Neufeld, P. Marszal, J. Gren, G. Smith, S. Jones, R. Proulx, Y. Deschambault, et al. 2004. Immunization with modified vaccinia virus Ankara-based recombinant vaccine against severe acute respiratory syndrome is associated with enhanced hepatitis in ferrets. *J. Virol.* 78: 12672–12676.
48. Czub, M., H. Weingartl, S. Czub, R. He, and J. Cao. 2005. Evaluation of modified vaccinia virus Ankara based recombinant SARS vaccine in ferrets. *Vaccine* 23: 2273–2279.
49. Corapi, W. V., C. W. Olsen, and F. W. Scott. 1992. Monoclonal antibody analysis of neutralization and antibody-dependent enhancement of feline infectious peritonitis virus. *J. Virol.* 66: 6695–6705.
50. Halstead, S. B. 1982. Immune enhancement of viral infection. *Prog. Allergy* 31: 301–364.
51. Deming, D., T. Sheahan, M. Heise, B. Yount, N. Davis, A. Sims, M. Suthar, J. Harkema, A. Whitmore, R. Pickles, et al. 2006. Vaccine efficacy in senescent mice challenged with recombinant SARS-CoV bearing epidemic and zoonotic spike variants. *PLoS Med.* 3:e525.
52. Boelen, A., A. Andeweg, J. Kwakkel, W. Lokhorst, T. Bestebroer, J. Dormans, and T. Kimman. 2000. Both immunisation with a formalin-inactivated respiratory syncytial virus (RSV) vaccine and a mock antigen vaccine induce severe lung pathology and a Th2 cytokine profile in RSV-challenged mice. *Vaccine* 19: 982–991.
53. Johnson, T. R., J. E. Johnson, S. R. Roberts, G. W. Wertz, R. A. Parker, and B. S. Graham. 1998. Priming with secreted glycoprotein G of respiratory syncytial virus (RSV) augments interleukin-5 production and tissue eosinophilia after RSV challenge. *J. Virol.* 72: 2871–2880.
54. Jin, H., C. Xiao, Z. Chen, Y. Kang, Y. Ma, K. Zhu, Q. Xie, Y. Tu, Y. Yu, and B. Wang. 2005. Induction of Th1 type response by DNA vaccinations with N, M, and E genes against SARS-CoV in mice. *Biochem. Bhiophys. Rex. Commun.* 328: 979–986.
55. Shi, S. Q., J. P. Peng, Y. C. Li, C. Qin, G. D. Liang, L. Xu, Y. Yang, J. L. Wang, and Q. H. Sun. 2006. The expression of membrane protein augments the specific responses induced by SARS-CoV nucleocapsid DNA immunization. *Mol. Immunol.* 43: 1791–1798.
56. Faber, M., E. W. Lamirande, A. Roberts, A. B. Rice, H. Koprowski, B. Dietzschold, and M. J. Schnell. 2005. A single immunization with a rhabdovirus-based vector expressing severe acute respiratory syndrome coronavirus (SARS-CoV) S protein results in the production of high levels of SARS-CoV-neutralizing antibodies. *J. Gen. Virol.* 86: 1435–1440.
57. Du, L., G. Zhao, Y. Lin, H. Sui, C. Chan, S. Ma, Y. He, S. Jiang, C. Wu, K. Y. Yuen, et al. 2008. Intranasal vaccination of recombinant adeno-associated virus encoding receptor-binding domain of severe acute respiratory syndrome coronavirus (SARS-CoV) spike protein induces strong mucosal immune responses and provides long-term protection against SARS-CoV infection. *J. Immunol.* 180: 948–956.

Suppression of an Already Established Tumor Growing through Activated Mucosal CTLs Induced by Oral Administration of Tumor Antigen with Cholera Toxin[1]

Ayako Wakabayashi, Yohko Nakagawa, Masumi Shimizu, Keiichi Moriya, Yasuhiro Nishiyama, and Hidemi Takahashi[2]

Priming of CTLs at mucosal sites, where various tumors are originated, seems critical for controlling tumors. In the present study, the effect of the oral administration of OVA plus adjuvant cholera toxin (CT) on the induction of Ag-specific mucosal CTLs as well as their effect on tumor regression was investigated. Although OVA-specific TCRs expressing lymphocytes requiring in vitro restimulation to gain specific cytotoxicity could be detected by OVA peptide-bearing tetramers in both freshly isolated intraepithelial lymphocytes and spleen cells when OVA was orally administered CT, those showing direct cytotoxic activity without requiring in vitro restimulation were dominantly observed in intraepithelial lymphocytes. The magnitude of such direct cytotoxicity at mucosal sites was drastically enhanced after the second oral administration of OVA with intact whole CT but not with its subcomponent, an A subunit (CTA) or a B subunit (CTB). When OVA plus CT were orally administrated to C57BL/6 mice bearing OVA-expressing syngeneic tumor cells, E.G7-OVA, in either gastric tissue or the dermis, tumor growth was significantly suppressed after the second oral treatment; however, s.c. or i.p. injection of OVA plus CT did not show any remarkable suppression. Those mucosal OVA-specific CTLs having direct cytotoxicity expressed CD8$\alpha\beta$ but not CD8$\alpha\alpha$, suggesting that they originated from thymus-educated cells. Moreover, the infiltration of such OVA-specific CD8$^+$ CTLs was observed in suppressed tumor tissues. These results indicate that the growth of ongoing tumor cells can be suppressed by activated CD8$\alpha\beta$ CTLs with tumor-specific cytotoxicity via an orally administered tumor Ag with a suitable mucosal adjuvant. *The Journal of Immunology,* **2008, 180: 4000–4010.**

Many malignant tumors originate from various epithelial tissues such as the skin or mucosal sites such as the esophagus, stomach, colon, or lung (1). Thus, as a cancer vaccine, it is essential to stimulate mucosal or dermal immune systems, as well as the systemic immune system, with a suitable Ag, adjuvant, and administration route as reviewed by Finn (2). Mucosal immunization using an adjuvant that enables the priming of both mucosal and systemic immunity (3, 4) may be a good way to prevent or treat mucosal tumors. In particular, the induction of mucosal CTLs that can specifically recognize tumor-derived peptide Ags presented by the corresponding class I MHC molecules seems to be one of the most important issues for eliminating tumor cells (5).

In the mucosal compartment, lymphocytes located in the intestinal epithelium are almost exclusively T cells called intraepithelial lymphocytes (IELs)[3] (3). Such IELs are mostly CD8$^+$ T cells that are classified into three distinct populations: TCR$\alpha\beta^+$CD8$\alpha\beta^+$, TCR$\alpha\beta^+$CD8$\alpha\alpha^+$, and TCR$\gamma\delta^+$CD8$\alpha\alpha^+$ (6). IELs contain cytotoxic properties and specifically eliminate virus- or parasite-infected cells (7–9); however, although spontaneous cytotoxicity of human IELs against tumor cells has been reported (10, 11), their actual specificity on tumors is still unknown. Recently, we have reported (12) that a marked increase in the number of HIV-1-specific CD8$\alpha\beta$-positive T cells among IELs was observed in HIV-1-specific TCR transgenic (Tg) mice when they received intrarectal or i.p. administration of the recombinant vaccinia virus (rVV) expressing a known restricted CTL epitope, P18 (rVV-P18), which is restricted by H-2D^d-class I MHC molecules (13). Using H-2D^d/P18 tetramers, we could detect CD8-positive, P18-specific TCR-expressing T cells in freshly isolated IELs and splenic T cells of unchallenged naive Tg mice. Although those H-2D^d/P18 tetramer-positive CD8 T cells from naive Tg mice did not show any specific cytotoxicity, freshly isolated mucosal T cells bearing CD8$\alpha\beta$ but not CD8$\alpha\alpha$ from activated Tg mice with rVV-P18 represented P18-specific cytotoxicity against tumor cells expressing the epitope, and the magnitude of cytotoxicity was much stronger than that in activated splenic T cells (12). These results suggest that in vivo activated mucosal CD8$\alpha\beta$ CTLs with tumor-specific cytotoxicity may be critical for controlling tumors expressing the specific epitope in vivo rather than systemic splenic CTLs.

Cholera toxin (CT) derived from *Vibrio cholerae* is known as a potent mucosal adjuvant comprised of one toxic A subunit (CTA) with ADP-ribosyltransferase activity and five nontoxic B subunits (CTB) responsible for binding to monosialoganglioside (GM) 1 on the cell surface (14, 15). CT adjuvant helps to produce both systemic IgG and mucosal IgA (16) as well as to induce Ag-specific

Department of Microbiology and Immunology, Nippon Medical School, Tokyo, Japan

Received for publication April 13, 2007. Accepted for publication January 7, 2008.

The costs of publication of this article were defrayed in part by the payment of page charges. This article must therefore be hereby marked *advertisement* in accordance with 18 U.S.C. Section 1734 solely to indicate this fact.

[1] This work was supported in part by Grants-in-Aid for Young Scientists from the Japan Society for the Promotion of Sciences, from the Ministry of Education, Science, Sport, and Culture, from the Ministry of Health and Labor and Welfare, Japan, and from the Promotion and Mutual Aid Corporation for Private Schools of Japan.

[2] Address correspondence and reprint requests to Dr. Hidemi Takahashi, Department of Microbiology and Immunology, Nippon Medical School, 1-1-5 Sendagi, Bunkyo-ku, Tokyo 113-8602, Japan. E-mail address: htkuhkai@nms.ac.jp

[3] Abbreviations used in this paper: IEL, intraepithelial lymphocyte; CT, cholera toxin; CTA, CT A subunit (toxic); CTB, CT B subunit (nontoxic); DC, dendritic cell; GM, monosialoganglioside; *Hp*, *Helicobacter pylori*; LPL, lamina propria lymphocyte; MadCAM-1, mucosal addressin cell-adhesion molecule-1; OVA-CT, CT-conjugated OVA; PP, Peyer's patch; rVV, recombinant vaccinia virus; SC, spleen cell; Tg, transgenic; TIL, tumor-infiltrating lymphocyte.

$CD4^+$ T cell responses in the spleen, reflecting the systemic compartment, and in Peyer's patches (PPs), reflecting the mucosal compartment (17). In addition, it has been demonstrated (18) that OVA-specific CTLs could be primed in C57BL/6 mice following oral exposure to a combination of OVA with CT, and specific cytotoxic activity was detected from spleen cells (SCs) only when they were restimulated in vitro with irradiated OVA-expressing syngeneic tumor cells, E.G7-OVA, which are OVA gene-transfected EL4 thymoma cells (19, 20). Also, intranasal preimmunization with OVA peptide (SIINFEKL) plus CT primed similar OVA-specific CTLs in the spleen of C57BL/6 mice, and the immunized mice were protected from the development of transferred E.G7-OVA (21).

Moreover, it has been shown that adoptive transfer of naive $CD8^+$ OVA-specific OT-I T cells into E.G7-OVA tumor-bearing syngeneic mice did not inhibit tumor growth, although adoptive transfer of preactivated OT-I CTL in vitro inhibited tumor growth in a dose-dependent manner (22). Furthermore, it has recently been reported that vaccination with dendritic cells (DCs) prepulsed ex vivo with CT-conjugated OVA (OVA-CT) gave rise to OVA-specific splenic $CD8^+$ T cells that produced IFN-γ, were cytotoxic to E.G7-OVA cells in vivo, and rejected already established in vivo E.G7-OVA tumors associated with high numbers of tumor-infiltrating $CD8^+$ T cells (23), indicating that the elimination of previously established tumor cells might require the infiltration of tumor-specific activated $CD8^+$ CTLs.

In the present study, we found two distinct types of $CD8\alpha\beta$-positive T cells among freshly isolated lymphocytes expressing OVA-specific TCRs, which can be detected by OVA peptide-bearing tetramers. One is in an activated effector state with cytotoxic activity and the other is a resting state and may gain cytotoxicity when stimulated with an OVA epitope peptide in vitro. Based on the observations, we defined direct cytotoxicity as the former state, in which freshly isolated and unstimulated CD8 T cells had specific cytotoxicity. Therefore, by comparing systemic SCs, we asked whether OVA-specific cytotoxic activity could be observed among freshly isolated IELs in mice orally administered OVA plus CT and examined whether those activated CTLs would reject or suppress the growth of already established tumors. Consequently, we observed dominant $TCR\alpha\beta$ and $CD8\alpha\beta$ OVA-specific CTL activities in freshly isolated IELs rather than in SCs after the oral administration of OVA plus CT, and such mucosal CTL activities could be expanded after oral boosting. Moreover, the growth of E.G7-OVA inoculated into the stomach or the epidermis was significantly suppressed, accompanied by the expansion of activated mucosal CTLs, and the infiltration of such OVA-specific $CD8\alpha\beta^+$ CTLs was observed in suppressed dermal tumor tissues. These results indicate that the growth of ongoing tumor cells can be suppressed in vivo by activated $CD8\alpha\beta$ CTLs with tumor-specific cytotoxicity via an orally administered tumor Ag with a suitable mucosal adjuvant.

Materials and Methods

Mice

Six- to 8-wk-old female C57BL/6 ($H\text{-}2^b$) mice were purchased from Charles River Japan, maintained in microisolator cages under pathogen-free conditions, and fed autoclaved laboratory chow and water. All animal experiments were performed according to guidelines for the care and use of laboratory animals set by the National Institutes of Health (NIH; Bethesda, MD) and approved by the Review Board of Nippon Medical School (Tokyo, Japan).

Oral and systemic immunization

Chicken egg OVA, grade V (Sigma Aldrich), was dissolved in sterilized PBS. Mice were orally administered 100 mg of OVA or 10 μg of CT (List Biological Laboratories) alone or 100 mg of OVA plus 10 μg of CT, CTA, or CTB (List Biological Laboratories) in 0.3 ml of PBS. In some experiments, mice were orally administered 10 mg of OVA plus 10 μg of CT. For systemic immunization, mice were i.p. or s.c. injected with 100 mg of OVA or the same dose of OVA plus 10 μg of CT.

Preparation of IELs, lamina propria lymphocytes (LPLs), SCs, and tumor-infiltrating lymphocytes (TILs)

IELs were prepared by the method described previously (12). In brief, after the small intestine, large intestine, or stomach was obtained from mice, fecal materials were flushed from the lumen with HBSS (Invitrogen Life Technologies) and connective tissues were carefully removed. The obtained guts were inverted and cut into several segments that were transferred to a 50-ml conical tube (Becton Dickinson Labware) containing 45 ml of HBSS with 5% FCS, 100 U/ml penicillin (Invitrogen Life Technologies), and 100 μg/ml streptomycin (Invitrogen Life Technologies). The tube was then shaken at 37°C for 45 min (horizontal position; orbital shaker at 150 rpm). Harvested cells from the intestinal epithelium were passed through a 10-ml syringe column containing loosely packed glass wool to remove tissue debris. Subsequently, the cells were suspended in 30% Percoll solution (Amersham Biosciences) and centrifuged for 20 min at 1,800 rpm. Cells at the bottom of the solution were then subjected to Percoll discontinuous gradient centrifugation for 20 min at 1,800 rpm and IELs were recovered at the interphase of 44 and 70% Percoll solutions. LPLs were prepared by the method described previously (24). In brief, after the small intestine, large intestine, or stomach was dissected from mice, fecal material was flushed from the lumen with HBSS and PPs were carefully removed. The obtained guts were inverted and cut into several segments that were transferred to a 50-ml conical tube containing 45 ml of HBSS with 5% FCS and 1 mM EDTA (Wako Pure Chemical Industries). The tube was shaken at 37°C for 45 min (horizontal position; orbital shaker at 150 rpm). The gut segments were then washed with PBS and shaken in 40 ml of HBSS with 5% FCS and 0.1 mg/ml collagenase (Sigma-Aldrich) at 37°C for 45 min (horizontal position; orbital shaker at 60 rpm). Harvested cells were passed through a nylon mesh and suspended in 40% Percoll solution, and then 70% Percoll solution was underlain. The solution was centrifuged for 20 min at 1,800 rpm and LPLs were recovered at the interphase of 40 and 70% Percoll solutions. These procedures provided >95% viable lymphocytes with a cell yield of $5\text{–}10 \times 10^6$ of small intestinal IELs, $2\text{–}3 \times 10^5$ of large intestinal IELs, $7\text{–}12 \times 10^3$ of gastric IELs, $4\text{–}9 \times 10^5$ of small intestinal LPLs, $1\text{–}3 \times 10^5$ of large intestinal LPLs, or $5\text{–}9 \times 10^4$ of gastric LPLs per mouse. The cells were suspended in complete T cell medium (25) composed of RPMI 1640 medium (Sigma-Aldrich) supplemented with 2 mM L-glutamine (ICN Biomedicals), 1 mM sodium pyruvate (Invitrogen Life Technologies), 0.1 mM nonessential amino acid (Invitrogen Life Technologies), a mixture of vitamins (ICN Biomedicals), 1 mM HEPES (Invitrogen Life Technologies), 100 U/ml penicillin (Invitrogen Life Technologies), 100 μg/ml streptomycin (Invitrogen Life Technologies), 50 μM 2-ME (Sigma-Aldrich), and heat-inactivated 10% FCS. For TIL preparation, tumors were removed from mice, incubated in 1 mg/ml collagenase (Wako Pure Chemical Industries) with PBS at 37°C for 1 h, and crushed gently. TILs were prepared using Percoll solutions as described in the previous paragraph regarding IEL preparation. The spleen was aseptically removed and a single cell suspension was prepared. For osmotic hemolysis, single cells were suspended in 0.1× PBS and an equal amount of 2× PBS was added immediately. To enrich IELs, LPLs, and TILs from mice, the interface between the 40 and 70% Percoll solutions (26), in which NK cells and unfractionated SCs, which may also include NK cells, must be included, was collected.

Flow cytometry analysis

Cells were double-stained with PE-labeled $H\text{-}2K^b$/OVA tetramer-SIINFEKL (Beckman Coulter) or $H\text{-}2K^b$/PB1 tetramer-SSYRRPVGI (Medical & Biological Laboratories) and FITC-labeled anti-mouse TCRβ, CD8α (BD Pharmingen), or CD8β (Caltag Laboratories). Peptide PB1 703–711, SSYRRPVGI, for the control tetramer was derived from influenza virus (27). Dead cells were determined using 7-aminoactinomycin D viability dye (Beckman Coulter) and stained cells were analyzed by FACScan using the CellQuest program (BD Biosciences).

In vitro restimulation of SCs or IELs with E.G7-OVA

Lymphocytes were restimulated in vitro by the method described previously (19). Freshly isolated SCs (3×10^7) or IELs (3×10^7) were restimulated with 3×10^6 irradiated (20,000 rad) E.G7-OVA cells (19, 20) ($H\text{-}2^b$; American Type Culture Collection) in 10 ml of complete T cell medium per upright 25-cm^2 flask in 5% CO_2 at 37°C for 6 days. Six days later, the viability of the lymphocytes was 35–51% in SCs and 16–26% in IELs. The

in vitro restimulated cells were collected and their OVA-specific cytotoxicity was measured by the following procedure.

CTL assay

For the CTL assay, freshly isolated IELs, SCs, or TILs were used. Cytolytic activity was measured using a standard ^{51}Cr-release assay as previously described (12). In brief, various numbers of effector cells were incubated with 3×10^3 ^{51}Cr-labeled targets for 6 h at 37°C in 200 μl of RPMI 1640 medium containing 10% FCS in round-bottom 96-well cell culture plates (BD Biosciences). After incubation, the plates were centrifuged for 10 min at 330 × *g*, and 100 μl of cell-free supernatants were collected to measure radioactivity with a Packard Auto-Gamma 5650 counter (Hewlett-Packard Japan). Maximum release was determined from the supernatant of cells that had been lysed by the addition of 5% Triton X-100, and spontaneous release was determined from target cells incubated without added effector cells. The percentage of specific lysis was calculated as 100 × (experimental release − spontaneous release)/(maximum release − spontaneous release). SEs of the means of triplicate cultures were always <5% of the mean. Each experiment was performed at least three times.

Measurement of in vivo antitumor effects

E.G7-OVA cells (5×10^6), OVA gene-transfected EL4 thymoma cells (19, 20), were implanted into the gastric or dermal tissue of syngeneic C57BL/6 mice (H-2^b). For tumor implantation into the gastric tissue, mice were anesthetized and underwent an abdominal operation and then E.G7-OVA cells in 50 μl of RPMI 1640 were injected into the muscle layer of the stomach using a syringe with a 29-gauge needle (Terumo). For implantation into the dermal tissue, mice were anesthetized and E.G7-OVA cells in 100 μl of RPMI 1640 were injected intradermally by a 29-gauge needle syringe. On day 3 after implantation into the gastric or dermal tissue, when the tumor mass became visible, tumor-bearing mice were orally or systemically administered OVA plus CT as described above. Seven days after the first administration, some of the mice were similarly boosted with the same materials. The growing tumors implanted into the gastric or dermal tissues were followed by measuring the length (*a*) and width (*b*), the and tumor volume (*V*) was calculated according to the formula $V = ab^2/2$ as reported previously (28). When the longer axis of each tumor was >20 mm, all mice were anesthetized and sacrificed according to the guidelines for the care and use of laboratory animals set by the NIH.

Histological analysis of tumor tissues

Freshly excised tumor tissues were embedded in Tissue-Tek OCT compound (Sakura Finetek) at −80°C. Tissue segments were sectioned at 6 μm using a cryostat. Sections were placed on a poly-L-lysine-coated glass slide, air dried, and then fixed in 10% formalin PBS for 5 min and stained with H&E. For immunohistochemical staining, sections were fixed in cold acetone for 5 min and incubated with blocking solution (Block-ace; Dainippon Pharmaceutical) for 30 min at 37°C and then incubated with biotin-conjugated rat anti-CD8β Ab (Caltag Laboratories) or control isotype-matched rat IgG2a Ab (Caltag Laboratories) overnight at 4°C. Endogenous peroxidase was quenched by incubation in 0.3% H_2O_2 and 0.1% NaN_3 in distilled water for 10 min. The sections were incubated with avidin-biotin peroxide complexes (Vectastain ABC kit; Vector Laboratories) followed by color reaction with a Vectastain diaminobenzidine substrate kit (Vector Laboratories).

Statistical analysis

Student's *t* test was used to determine the statistical significance of differences between groups in tumor growth. Data were considered significant at $p < 0.05$.

Results

Priming of OVA-specific CD8αβ-positive CTLs with direct cytotoxicity via oral administration with OVA plus CT

It has been reported that OVA-specific CTLs could be primed in C57BL/6 mice by oral or i.v. immunization with OVA plus CT together with nontoxic CTB, and specific cytotoxic activity was detected from immune SCs only when they were restimulated in vitro with irradiated OVA-expressing syngeneic tumor (E.G7-OVA) cells (18). It has also been shown that activated CTLs but not naive primed CTLs could represent antitumor responses in vivo (22). Similarly, we have recently observed in HIV-1-specific CTL-TCR transgenic mice that activated CTLs but not freshly isolated TCR-bearing CD8αβ-positive T cells showed specific cytotoxicity, and the most critical sites for activating TCR-bearing CD8αβ T cells were mucosal compartments when Tg mice were administered a specific Ag for TCR (12).

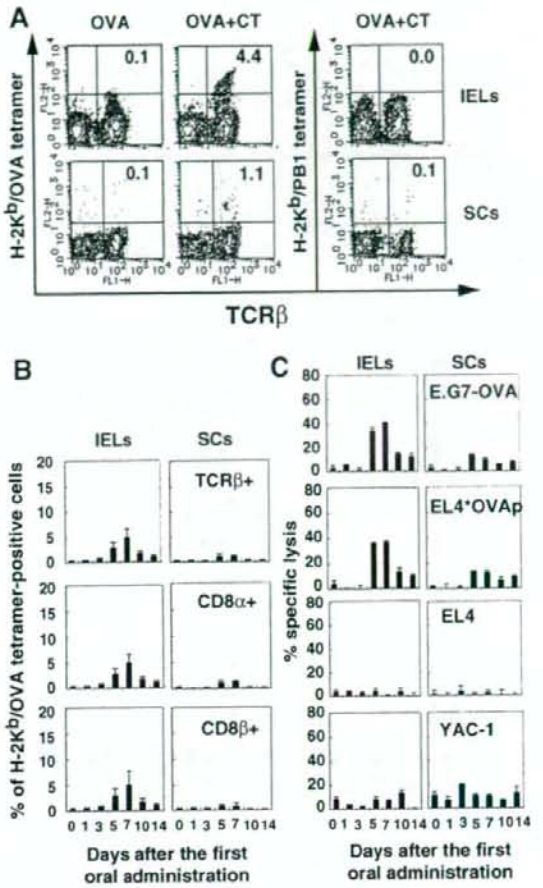

FIGURE 1. Analysis of OVA-specific direct cytotoxicities in IELs and SCs after primary immunization with OVA plus CT. *A*, Analysis of H-2K^b/OVA tetramer-positive cells. C57BL/6 mice were orally administered OVA or OVA plus CT once. IELs and SCs were collected from mice 5 days after the first oral administration, stained with either PE-labeled H-2K^b/OVA tetramer-SIINFEKL or H-2K^b/PB1 tetramer-SSYRRPVGI together with FITC-labeled anti-mouse TCRβ, and analyzed by flow cytometry. Each value represents the percentage of cells expressing both indicated markers. Data are representative of three independent experiments. *B*, Kinetics of H-2K^b/OVA tetramer-positive cells after primary immunization. C57BL/6 mice were orally administered OVA plus CT once. IELs and SCs were collected from mice at various days after the first oral administration, stained with PE-labeled H-2K^b/OVA tetramer together with FITC-labeled anti-mouse TCRβ, CD8α, or CD8β, and analyzed by flow cytometry. The results are shown as the mean ± SD of four mice. *C*, Kinetics of OVA-specific direct cytotoxic responses. C57BL/6 mice were orally primed and cells were collected as described in *B*. OVA-specific CTL responses were measured by ^{51}Cr-release assay using E.G7-OVA cells (H-2^b), YAC-1 cells, and EL4 cells (H-2^b) pulsed with or without 4 μM OVA-peptide, SIINFEKL, as target cells. E:T ratio was 100:1. The results shown as the mean ± SD in triplicate of pooled cells from two mice are representative of three independent experiments.

These findings prompted us to examine whether direct OVA-specific cytotoxic activity could be induced among IELs in mice

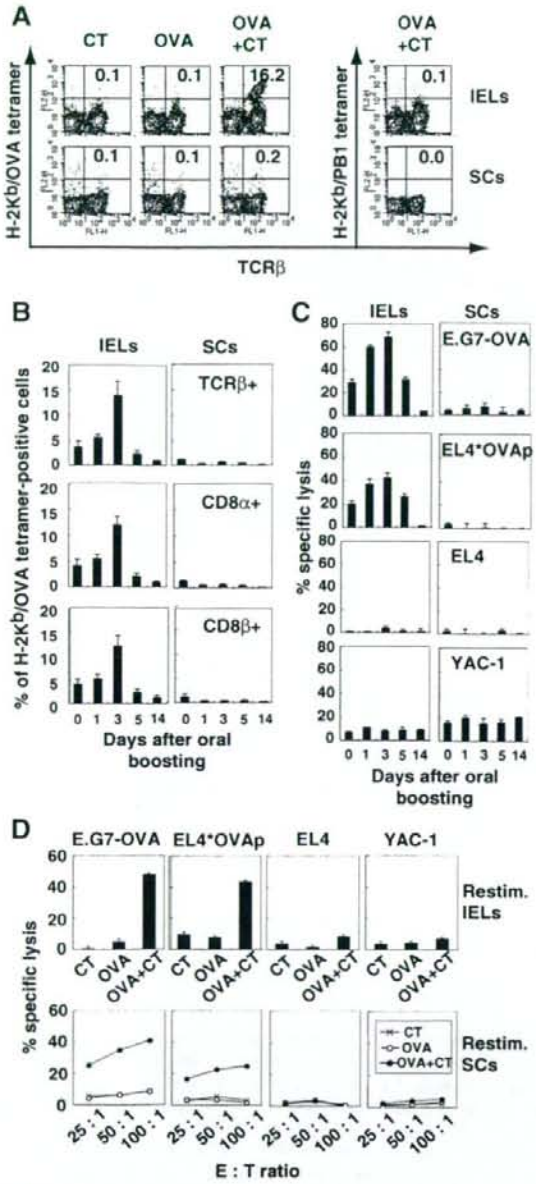

FIGURE 2. Expansion of direct OVA-specific cytotoxicities after oral boosting with OVA plus CT. *A*, Activated H-2K^b/OVA tetramer-positive cells after oral boosting. C57BL/6 mice were orally administered CT, OVA, or OVA plus CT once weekly for 2 wk. IELs and SCs were collected from mice 3 days after the second oral boost and stained with PE-labeled H-2K^b/OVA tetramer or H-2K^b/PB1 tetramer together with FITC-labeled anti-mouse TCRβ. Each value represents the percentage of cells expressing both indicated markers. Data are representative of three independent experiments. *B*, Kinetics of H-2K^b/OVA tetramer-positive cells after oral boosting. C57BL/6 mice were orally administered OVA plus CT once weekly for 2 wk. IELs and SCs were collected from mice at various days after the second oral boost, stained with PE-labeled H-2K^b/OVA tetramer together with FITC-labeled anti-mouse TCRβ, CD8α, or CD8β, and analyzed by flow cytometry. The results are shown as the mean ± SD of four mice. *C*, Kinetics of the secondary expansion of OVA-specific direct CTL responses. C57BL/6 mice were treated orally and the cells were collected as described in *B*. OVA-specific CTL responses were measured by ^{51}Cr-release assay using E.G7-OVA cells, YAC-1 cells, and EL4 cells pulsed with or without OVA peptide as targets. The E:T ratio is 100:1. The results shown as the mean ± SD in triplicate of pooled cells from two mice are representative of three independent experiments. *D*, Activation of OVA-specific CTLs by in vitro restimulation (Restim.). C57BL/6 mice were orally administered CT, OVA, or OVA plus CT once weekly for 2 wk. IELs (3×10^7) and SCs (3×10^7) were collected from mice 9 days after the second oral boost, and cocultured with 3×10^6 irradiated E.G7-OVA. Six days later, OVA-specific lysis of stimulated IELs and SCs was measured by ^{51}Cr-release assay. The E:T ratio is 100:1 in IELs and 100:1, 50:1, or 25:1 in SCs. The results are shown as the mean ± SD in IELs or the mean in SCs in triplicate of pooled cells from two mice. Data are representative of three independent experiments.

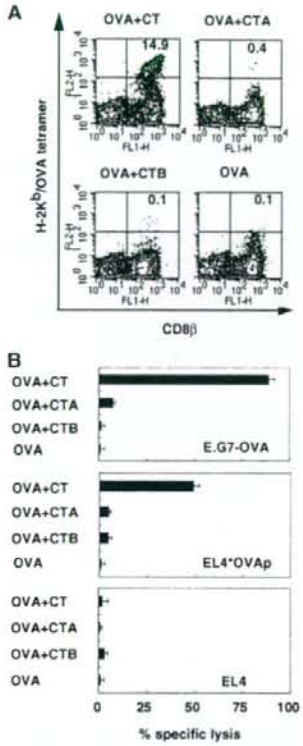

FIGURE 3. Both subunits, CTA and CTB, are essential for the induction of OVA-specific CTLs. C57BL/6 mice were orally administered OVA or OVA plus intact CT, CTA subunit or CTB subunit once weekly for 2 wk. IELs were collected from mice 3 days after the second oral administration. *A*, IELs were stained with PE-labeled H-2K^b/OVA tetramer and FITC-labeled anti-mouse CD8β. Each value represents the percentage of cells expressing both indicated markers. *B*, OVA-specific CTL responses of isolated IELs were measured by ^{51}Cr-release assay using E.G7-OVA cells, EL4 cells pulsed with or without OVA peptide as targets. The E:T ratio is 100:1. Data are shown as the mean ± SD in triplicate of pooled cells from two mice. The results are representative of three independent experiments for both *A* and *B*.

administered OVA plus CT orally without requiring in vitro restimulation. To carry out this experiment, we used a H-2K^b/OVA tetramer to detect cells expressing OVA-specific TCR in freshly isolated IELs as well as in the SCs of primed mice 5 days after immunization. Also, to evaluate the purity of IELs, CD103 (integrin

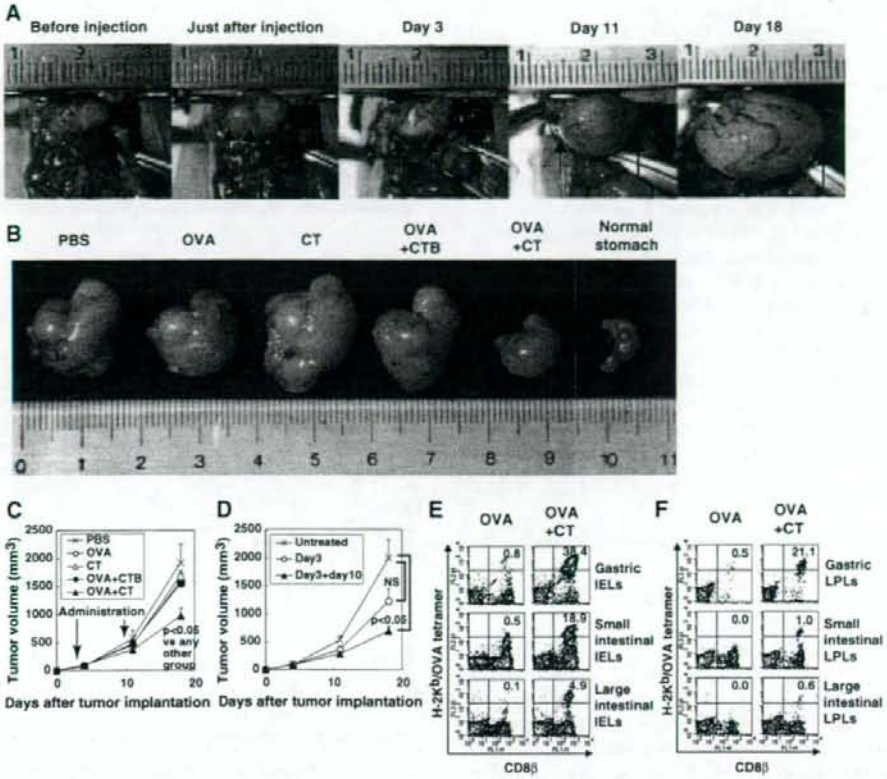

FIGURE 4. Suppression of the growth of a tumor implanted into gastric tissue by oral administration of OVA plus CT. *A*, Growth of visible tumor after implantation of E.G7-OVA cells into gastric tissue. C57BL/6 mice were implanted with 5×10^6 E.G7-OVA cells into the muscle layer of the stomach. Each day, the same mice were anesthetized and underwent an abdominal operation, and tumors were observed. Arrows point to both ends of the longer axis in the tumor. *B*, C57BL/6 mice were implanted with 5×10^6 E.G7-OVA cells into the muscle layer of the stomach. Three days later, tumor-bearing mice were orally administered PBS, OVA, CT, OVA plus CTB subunit, or OVA plus CT. Seven days later, the second oral administration was performed in the same manner. Stomachs were excised from the mice 18 days after tumor implantation, as well as from untreated, normal mice. *C*, Tumor volumes were calculated based on the formula described in *Materials and Methods*, and the results are shown as the mean ± SEM. The results were obtained from 9–13 mice per group. $p < 0.05$ indicates statistically significant difference between OVA plus CT (▲) and any other groups. *D*, C57BL/6 mice were implanted with E.G7-OVA cells in the stomach. Three days later, tumor-bearing mice were orally administered OVA plus CT or left untreated. Seven days later, some orally immunized mice were boosted in the same manner or left untreated. The results are shown as the mean ± SEM of 5–7 mice per group. $p < 0.05$ and NS indicate statistically significant and not significant differences, respectively, between the boosted (▲) and nonboosted (○) groups and the untreated group (×). *E* and *F*, Induction of CD8β and H-2K^b/OVA tetramer-positive cells in IELs (*E*) and LPLs (*F*) of the stomach, small intestine, or large intestine after oral administration of OVA plus CT. C57BL/6 mice were orally administered OVA or OVA plus CT once weekly for 2 wk. IELs and LPLs were collected from mice 3 days after the second oral administration. Cells were stained with PE-labeled H-2K^b/OVA tetramer and FITC-labeled anti-mouse CD8β. Each value represents the percentage of cells expressing both indicated markers. The results are representative of three independent experiments.

α-IEL chain)-positive cells in the collected samples were examined by flow cytometry. CD103 is highly expressed on >90% of IELs (29, 30) but on only 15% of SCs (31). In the present study, CD103-positive cells occupied >90% of IELs and ~15% of SCs (data not shown). Although a small number of OVA-specific TCR-expressing cells were detected in both IELs (4.5–5.0%) and SCs (1.0–1.5%) after oral administration of OVA plus CT in comparison with control H-2K^b/PB1-positive cells, H-2K^b/OVA tetramer-positive cells were not observed in mice treated with OVA alone (Fig. 1*A*). Such OVA peptide-specific TCR-expressing cells were TCRγδ negative (data not shown) and both CD8α and β positive (Fig. 1*B*). The number of tetramer-positive cells, to which the magnitude of direct OVA-specific cytotoxicity closely corresponded, was maximal at day 7 after oral immunization with both IELs and SCs (Fig. 1*B*), but it did not correspond to NK cell activity as measured against YAC-1 targets (Fig. 1*C*). The results clearly demonstrate that direct OVA-specific CTL cytotoxicity is dominantly observed in mucosal IELs after primary oral administration of OVA plus CT.

Augmentation and kinetics of direct OVA-specific cytotoxicity by CD8αβ CTLs among IELs and SCs via oral boosting with OVA plus CT at day 7 after the primary administration

As shown above, because only 4.5–5.0% of IELs were temporarily activated by a one-shot oral administration, we extensively examined the effect of oral boosting with OVA plus CT at various days after primary immunization. The number of H-2K^b/OVA tetramer-positive cells was significantly enhanced among IELs but not among SCs when primed mice were boosted (Fig. 2*A*). Such an effect was highest when mice were boosted at day 7 after initial

priming (data not shown). Tetramer-positive cells were again TCRβ-, CD8α-, and CD8β-positive IELs and their number peaked at day 3 after boosting (Fig. 2*B*). Correspondingly, direct OVA-specific cytotoxicity was greatly enhanced among IELs and the maximal cytotoxicity of IELs was observed at day 3 after boosting (Fig. 2*C*), although such direct cytotoxicity appeared to be completely lost in SCs (Fig. 2*C*). Nonetheless, SCs showed good epitope-specific cytotoxicity similar to that of IELs when they were restimulated in vitro with irradiated E.G7-OVA (Fig. 2*D*), suggesting that the priming effect by the oral administration of OVA plus CT also remained in systemic SCs.

It should be noted that the memory of OVA-specific CTLs persisted among IELs but not SCs. When secondary boosting with OVA plus CT was performed even 6 mo after primary boosting at day 7, the number of H-2K^b/OVA tetramer-positive cells was still detected at ~6% in IELs, and they showed remarkable direct cytotoxicity of ~84.5% against E.G7-OVA cells and 58.4% against EL4 cells pulsed with OVA peptide 3 days after secondary boosting (data not shown). Again, we could not detect any measurable direct cytotoxicity in the SCs of secondary boosted mice (data not shown).

Both CTA and CTB subunits are required to induce direct OVA-specific cytotoxicity in IELs

CT is comprised of a single A subunit, CTA, and five B subunits, CTB. When OVA was administered orally to mice with either 10 μg of CTA or an equal amount of CTB, H-2K^b/OVA tetramer-positive cells as well as direct OVA-specific cytotoxicity could not be detected in IELs (Fig. 3, *A* and *B*) and SCs (data not shown), although a significant number of tetramer-positive cells and strong direct OVA-specific cytotoxicity were observed among IELs of mice administered orally with OVA plus 10 μg of intact CT (Fig. 3, *A* and *B*). Even when using 50 μg of CTA or CTB for the administration of OVA, direct cytotoxicity was not observed (data not shown); therefore, both CTA and CTB subunits are required to induce direct Ag-specific cytotoxicity.

Effects of oral administration and booting with OVA plus CT on OVA-expressing tumor growth established in the stomach

We then examined in vivo antitumor effects of oral administration with tumor Ag plus CT on already established tumors growing in mice. C57BL/6 mice were implanted with 5×10^6 syngeneic E.G7-OVA cells into the muscle layer of the stomach (Fig. 4*A*). Three days later, tumor-bearing mice (Fig. 4*A*) were orally administered various combinations of OVA plus adjuvant and boosted with the same materials 7 days after the initial oral administration. To our surprise, tumor growth in the stomach of mice orally administered OVA plus CT twice was visually (Fig. 4*B*) and significantly ($p < 0.05$; Fig. 4*C*) suppressed on day 18 after tumor implantation as compared with other control groups such as OVA plus CTB or CT alone. However, when tumor-bearing mice were orally administered OVA plus CT once and without boosting, no statistically significant suppression was observed on day 18 as compared with untreated control mice, although a slight suppressive effect could be seen (Fig. 4*D*). Therefore, two oral administrations of tumor-Ag plus CT with an appropriate interval induced significant ongoing tumor suppression.

As previously shown, direct OVA-specific cytotoxicity among small intestinal IELs was greatly enhanced after boosting with OVA plus CT (Fig. 2, *A*, *B*, and *C*). We also examined whether direct OVA-specific CTLs were induced in the IELs and LPLs of the stomach, small intestine, and large intestine from boosted mice in which gastric tumor growth was significantly suppressed. We observed an increase in the number of H-2K^b/OVA tetramer-positive

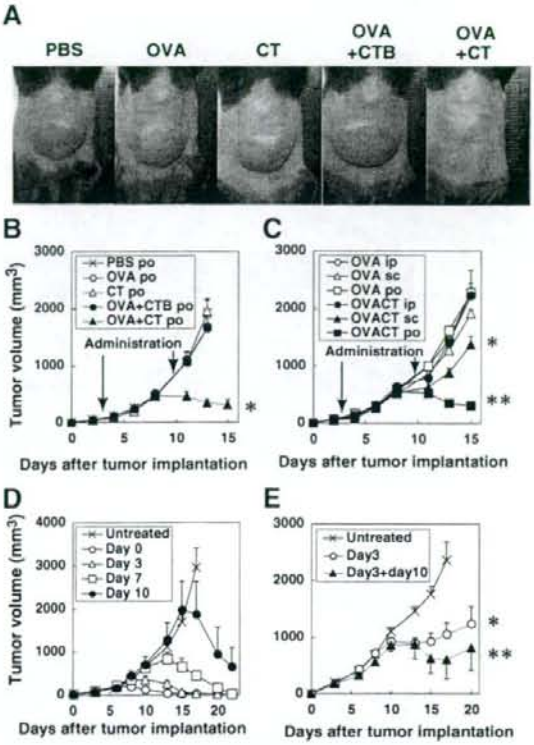

FIGURE 5. Suppression of intradermal tumor growth by oral administration with OVA plus CT. C57BL/6 mice were implanted intradermally with 5×10^6 E.G7-OVA cells. Three days later, tumor-bearing mice were orally administered PBS, OVA, CT, OVA plus CTB subunit, or OVA plus CT. Seven days later, the second oral administration was performed in the same manner. *A*, Visual suppressive effect of oral inoculation of OVA plus CT on dermal tumor growth. *B*, Tumor volumes were calculated based on the formula described in *Materials and Methods* and the results are shown as the mean ± SEM. Results were obtained from 5–6 mice per group. The asterisk (*) indicates statistically significant difference between the OVA plus CT group (closed triangle) and any other group at 11 days ($p < 0.05$) and 13 days ($p < 0.005$) after tumor inoculation. *C*, C57BL/6 mice were implanted intradermally with E.G7-OVA cells. Three days later, tumor-bearing mice were intraperitoneally (ip), subcutaneously (sc), or orally (po) administered OVA alone or OVA plus CT. Seven days later, the second treatment was performed in the same manner. The results are shown as the mean of tumor volumes ± SEM. Results were obtained from 5–6 mice per group. The asterisk (*) shows statistically significant differences ($p < 0.05$) between the s.c. OVA plus CT group (▲) and the s.c. OVA alone group at days 11, 13, and 15 after tumor implantation, and the two asterisks (**) indicate significant differences ($p < 0.01$) between the oral OVA plus CT group (■) and the oral OVA alone group on the same days. *D*, C57BL/6 mice were implanted intradermally with E.G7-OVA cells. The mice were orally administered once with OVA plus CT at day 0, 3, 7, or 10 after tumor implantation. The results are shown as the mean of tumor volumes ± SEM. Results were obtained from 10–12 mice per group. In single orally administered groups, significant tumor regression ($p < 0.05$) was observed at 7 days after oral administration compared with the untreated group. *E*, C57BL/6 mice were implanted intradermally with E.G7-OVA cells. Three days later, tumor-bearing mice were orally administered a low dose (10 mg) of OVA plus CT. Seven days later, some orally administered mice were boosted in the same manner. The results obtained from 5- mice per group are shown as the mean of tumor volumes ± SEM. The asterisk (*) indicates statistically significant differences ($p < 0.01$) between the nonboosted (○) and untreated mice (×) groups at days 15 and 17 after tumor implantation, and the two asterisks (**) indicate significant differences ($p < 0.005$) between the boosted (▲) and untreated groups on the same days.

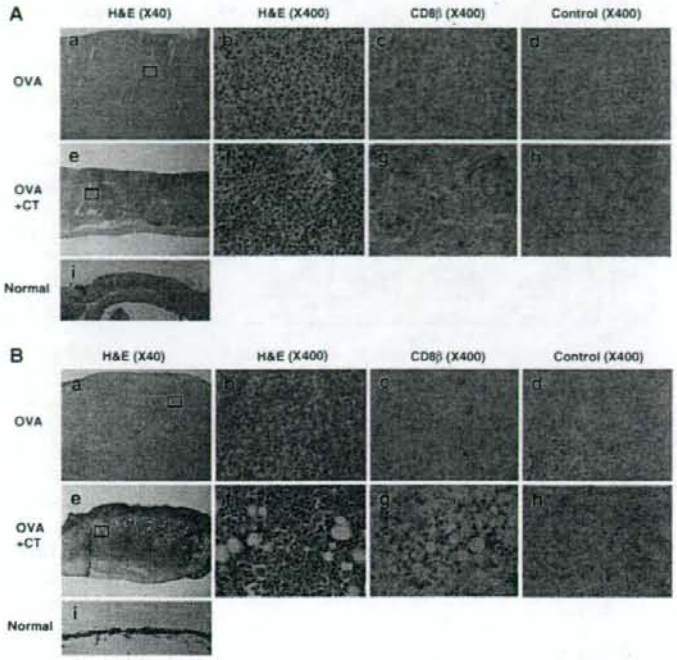

FIGURE 6. Infiltration of CD8$\alpha\beta$ positive lymphocytes into tumor tissues in mice orally administered OVA plus CT. C57BL/6 mice were implanted with 5×10^6 E.G7-OVA cells into the muscle layer of the stomach (*A*, *a–h*) or skin (*B*, *a–h*). Three days later, tumor-bearing mice were orally administered OVA (*A*, *a–d*, and *B*, *a–d*) or OVA plus CT (*A*, *e–h* and *B*, *e–h*). Seven days later, the second oral administration was performed in the same manner. Gastric and dermal tumor tissues were removed from mice 3 days after the second oral boost. Frozen sections of tumor tissues and normal tissues were prepared and stained with H&E (*A*, *a*, *b*, *e*, *f*, and *i* and *B*, *a*, *b*, *e*, *f*, and *i*) or immunohistochemically stained with biotin-conjugated rat anti-CD8β mAb (*A*, *c* and *g*, and *B*, *c* and *g*) or control isotype-matched rat IgG2a Ab (*A*, *d* and *h*, and *B*, *d* and *h*). Image magnification is either ×40 (*A*, *a*, *e*, and *i* and *B*, *a*, *e*, and *i*) or ×400 (*A*, *b–d* and *f–h* and *B*, *b–d* and *f–h*). *A*, *b* and *f* and *B*, *b* and *f* are enlarged images (×400) of the squared areas in the images (×40) of *A*, *a* and *e* and *B*, *a* and *e*, respectively.

cells among IELs in the stomach (38.4%) as well as the small (18.9%) and large intestine (4.9%) of tumor-suppressed mice (Fig. 4*E*) and also among LPLs in the stomach (21.1%) as well as the small (1.0%) and large (0.6%) intestine (Fig. 4*F*). Thus, the ability of LPLs to suppress tumor growth may be weaker than that of IELs. The results suggest that oral administration of Ag plus intact CT with appropriate mucosal boosting apparently suppressed the already established tumor growth in gastric tissue, particularly after oral boosting, probably through the activation of Ag-specific CTLs in the mucosal compartment.

Effects of oral administration and boosting with OVA plus CT on already established OVA-expressing dermal tumor growth

Next, we investigated the effect of the oral administration of tumor Ag plus CT on tumor growth in the skin, where the digestive tract is not directly associated. Mice were implanted with 5×10^6 E.G7-OVA cells intradermally. Three days later, tumor-bearing mice were orally administered various combinations of OVA plus adjuvant and boosted with the same materials 7 days after the initial oral administration. Interestingly, intradermal tumor growth was again strongly suppressed visually 11 days after tumor implantation in the dermis of mice orally administered OVA plus CT as compared with various other groups (Fig. 5*A*). This visual effect was confirmed by calculating the volume of the tumors established at day 11 and day 13 in each group ($p < 0.05$ and $p < 0.005$, respectively; Fig. 5*B*). We also examined the effect of the administration of tumor Ag plus CT via various routes on intradermal tumor growth. Although a slight suppression was observed by s.c. inoculation of OVA plus CT, tumor growth was not suppressed at all by i.p. administration in comparison with the oral treatment group (Fig. 5*C*). It should be noted that tumor growth in the dermis was markedly suppressed even by a single oral administration of OVA plus CT on day 0, 3, 7, or 10 after tumor implantation (Fig. 5*D*). In each group, tumor growth was suppressed ($p < 0.05$) and the tumor volume was small around 7 days after oral administration. Unexpectedly, there was almost no difference in the suppressive effects on tumor growth between mice treated with a single administration and boosted mice showing much stronger direct cytotoxicity (data not shown). However, when the dosage quantity of OVA was decreased by one-tenth, tumor growth in boosted mice was more significantly ($p < 0.005$) suppressed than in nonboosted mice ($p < 0.01$; Fig. 5*E*). Collectively, the results indicate that the oral administration of tumor Ag plus CT with appropriate mucosal boosting may induce a remarkable suppression of already established tumor growth in the skin via mucosally generated CTLs.

Infiltration of CD8$\alpha\beta$-positive cells in suppressed tumor tissues

We thus examined whether OVA-specific CD8$\alpha\beta$-positive CTLs were actually seen in suppressed tumor tissues such as the stomach and dermis. To determine tumor-infiltrating CD8$\alpha\beta^+$ cells, immunohistochemical staining was performed using biotin-conjugated rat anti-CD8β Ab (Fig. 6*A*, *c* and *g* and *B*, *c* and *g*) or control isotype-matched rat IgG2a Ab (Fig. 6*A*, *d* and *h* and *B*, *d* and *h*). Indeed, although mononuclear cells were seen in the gastric tumor tissues of mice treated with OVA alone, CD8$\alpha\beta$-positive cells were not observed at all (Fig. 6*A*, *a–d*). In contrast, infiltration of inflammatory mononuclear cells together with CD8$\alpha\beta$-positive cells was observed in suppressed gastric tumor tissues (Fig. 6*Ag*). As shown in Fig. 6*Ai*, normal gastric tissue is composed of the epithelium, lamina propria, lamina muscularis mucosae, muscle layer, and serosa from the inside surface in sequence. As compared with normal gastric tissue, a great number of large tumor cells (EG.7-OVA) were mainly found between the lamina muscularis mucosae and serosa of tumor-implanted tissues (Fig. 6*A*, *a* and *b*) and the infiltration of tumor cells into the lamina propria over the lamina muscularis mucosae was also observed (data not shown). However, in suppressed gastric tumor tissues (Fig. 6*Ae*) the tumor cell layer under the lamina muscularis mucosae was markedly thinner than that of an unsuppressed tumor (Fig. 6*Aa*), in which

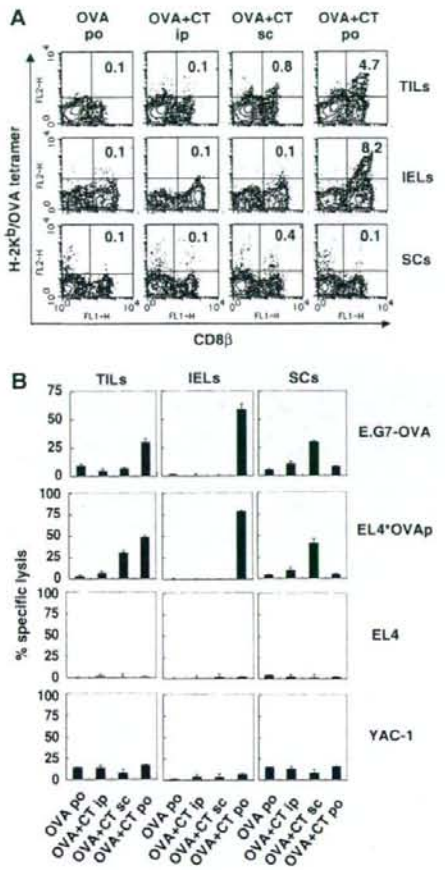

FIGURE 7. Detection of OVA-specific CTLs in TILs. C57BL/6 mice were implanted intradermally with E.G7-OVA cells. Three days later, mice were orally (po), subcutaneously (sc), or intraperitoneally (ip) administered OVA plus CT or orally treated with OVA. Seven days later, the second oral administration was performed in the same manner. TILs, IELs, and SCs were collected from mice 3 days after the second oral administration. *A*, TILs, IELs and SCs were double stained with PE-labeled H-2K^b/OVA tetramer and FITC-labeled anti-mouse CD8β. *B*, OVA-specific CTL responses of TILs, IELs, and SCs were measured by a ^{51}Cr-release assay using E.G7-OVA cells, YAC-1 cells, and EL4 cells pulsed with or without OVA peptide as targets. The E:T ratio is 5:1 in TILs, or 100:1 in IELs and SCs. The results are shown as the mean ± SD in triplicate of pooled cells from three mice. The results are representative of three independent experiments.

tumor cells almost never infiltrated the lamina propria over the lamina muscularis mucosae. Similarly, as for dermal tumor tissues, mononuclear cells together with CD8αβ-positive cells were not observed in mice treated with OVA alone (Fig. 6*B*, *a–d*), whereas the infiltration of a large number of mononuclear cells and CD8αβ-positive cells was observed in suppressed dermal tumor tissues (Fig. 6*B*, *e–g*). Dermal tumor sections were not stained with control isotype-matched rat IgG (Fig. 6*B*, *d* and *h*). As shown in Fig. 6*Bi*, normal skin is composed of epidermides and dermis from the surface in sequence. In tumor cell-implanted dermal tissues, although the infiltration of mononuclear cells or CD8αβ-positive cells was not observed, many large tumor cells were found thickly beneath the epidermides (Fig. 6*B*, *a* and *b*); however, when tumor cell-implanted mice were treated with OVA plus CT, most tumor cells became necrotic or apoptotic (Fig. 6*B*, *e* and *f*).

Measurement of tumor-specific cytotoxic activity by tumor-infiltrating cells in tumor-suppressed mice

To confirm whether infiltrated CD8αβ-positive T cells achieved OVA-specific cytotoxicity, we isolated TILs containing both mononuclear cells and CD8αβ-positive T cells from suppressed dermal tumor tissues as well as from their IELs and SCs. As expected, the number of H-2K^b/OVA tetramer-positive cells increased in both the TILs and IELs but not in the SCs of mice bearing suppressed tumors induced by oral administration with OVA plus CT as compared with mice inoculated with OVA plus CT via another route (Fig. 7*A*), and those increased tetramer-positive cells showed significant direct OVA-specific CTL activity (Fig. 7*B*). It should be noted that, although the number of increased cells specific for the H-2K^b/OVA tetramer was small in mice inoculated with OVA plus CT s.c., both the TILs (0.8%) and the SCs (0.4%) but not the IELs (0.1%) of the mice represented a detectable level of direct OVA-specific cytotoxicity (Fig. 7*B*). These findings suggest that s.c. immunization with Ag plus CT may preferably activate systemic (splenic) Ag-specific CTLs rather than local (intraepithelial) CTLs. Moreover, NK cell cytotoxicity determined against YAC-1 cells was not observed in TILs, IELs, and SCs by oral, s.c., or i.p. immunization of OVA plus CT (Fig. 7*B*), indicating that the suppression of tumor growth was mainly mediated by CD8αβ CTLs rather than by NK cell cytotoxicity.

Discussion

In the present study we demonstrated that when OVA plus intact CT was orally administered into mice, direct OVA-specific cytotoxicity was dominantly induced in IELs rather than SCs after the first oral priming, and direct OVA-specific cytotoxicity was remarkably expanded in IELs but not in SCs after oral boosting with the same doses of OVA plus CT. Such OVA-specific CTLs were thymic conventional K^b class I MHC molecule-restricted TCRαβ$^+$ CD8αβ T cells (32). Moreover, the growth of the OVA-expressing tumor E.G7-OVA thymoma, established previously either in the stomach or dermis, was significantly suppressed by the oral administration of OVA plus CT. Furthermore, marked infiltration of OVA-specific TCRαβ$^+$ CD8αβ CTLs with direct cytotoxicity in reduced tumor tissues was observed. These results suggest that activated CTLs with specific cytotoxicity generated at mucosal compartments by oral administration with OVA plus intact CT may be responsible for already established tumor regression.

The majority of tumor regression studies associated with activation of the immune system have focused on systemic immunity observed in the spleen, lymph nodes, and circulating blood rather than local mucosal immunity seen in gut IELs. Those studies have demonstrated only preventative results for tumor establishment by preadministration of tumor Ag plus a suitable adjuvant. In addition, to our knowledge only one study has been shown to suppress already established tumor growth by activating and expanding tumor infiltrating CD8$^+$ CTLs (23). In that study, i.v. vaccination with DCs prepulsed ex vivo with OVA-CT at day 3 and boosted at day 10 after OVA-expressing E.G7 tumor injection induced complete rejection of a visible tumor within 3 wk after the first treatment. Although the inoculation route and the materials for vaccination were different from ours, the timing of the priming and boosting to induce the suppression of already established tumor growth correlated exactly, suggesting that their methods may also initiate strong mucosal direct cytotoxicity mediated through CD8$^+$ CTLs.

Similar to our findings, they also showed that immunization with OVA-CT but not with CTB-conjugated OVA (OVA-CTB)-prepulsed DCs could successfully induce complete rejection of already established tumor growth, although OVA-CTB-prepulsed DC inoculation prevented tumor establishment but not ongoing tumor growth in the skin. Moreover, they insisted that OVA has to be coupled to CT and should be loaded onto DCs for therapeutic DC vaccination based on the observation that neither OVA-CT nor DCs pulsed with unconjugated OVA plus CT could prevent tumor progression. Nonetheless, our findings shown here apparently indicate that we were able to induce effective suppression of ongoing tumor growth by simple oral administration with unconjugated OVA and CT. These results suggest that we may control already established tumor growth at the surface compartments by activating mucosal $CD8^+$ CTLs via orally administered tumor Ag with a suitable mucosal adjuvant. Also, when OVA-CT is orally administered, the conjugation between OVA and CT may be broken through digestion by enzymes secreted in the gastrointestinal tract. Recently, we have reported that modification of OVA in the gastrointestinal tract is essential for oral tolerance induction against OVA (33). Therefore, it is possible that gastrointestinal digestion or modification of OVA may facilitate the delivery of OVA Ag into DCs, critical APCs for OVA-specific CTL induction.

For the efficient induction of such OVA-specific CTLs in vivo using DCs, Eriksson et al. have reported that OVA-CT-prepulsed DC immunization required at least two DC injections, reflecting the priming/boosting procedure (23); however, we have observed that a single oral administration of OVA plus CT seems sufficient to induce effective CTLs to prevent E.G7-OVA thymoma growth, particularly in the skin. This may be because mucosally activated CTLs through oral immunization may be more potent than systemically activated CTLs to suppress transplanted tumors at the mucosal compartment, and oral administration of OVA plus CT seems more efficient to induce mucosal CTLs than i.v. Ag-loaded DC inoculation. Further studies will be needed to explain the differences.

Although both CT-conjugated-OVA and CTB-conjugated OVA are cross-presented by MHC class I in DCs, only CT-OVA but not CTB-OVA cross-primes OVA-specific $CD8^+$ CTLs in vivo (23, 34). Additionally, DCs pulsed with intact OVA alone cannot cross-present and cross-prime CTLs (23). For the cross-priming of Ag-specific CTLs by Ag-captured immature DCs, maturation signaling via some surface molecules such as TLR-3 in those DCs is essential (35, 36). Although whole CT up-regulates the expression of MHC class II, B7.1, and B7.2 molecules on DCs in vitro, neither CTA nor CTB alone up-regulates the levels of surface markers on DCs (37, 38). Also, the binding of CTB to GM1 on DCs seems necessary to efficiently take up both CT itself and Ag and to induce cross-presentation by MHC class I molecules on DCs, whereas CTA may not be taken up to affect DCs. When DCs from GM1-lacking mice were matured in vitro, CT failed to up-regulate the expression of maturation markers and, thus, the binding of B subunits in CT to GM1 molecules on DCs is essential for the induction of DC maturation (37). It has been reported that CTA is required to not only assist in maturation but also to generate the migration of DCs (39, 40); therefore, CTB-mediated matured DCs can initiate their migration to secondary lymphoid organs and colocalization with naive T cells (38). Indeed, CT-loaded but not CTB-loaded DCs could migrate from marginal zones to T cell zones in the spleen (39) and from the subepithelial dome region to T cell zones in PPs (40); therefore, both CTA and CTB were essential for cross-priming CTLs in vivo and neither CTA nor CTB alone could induce CTLs at various compartments (Fig. 3). Taken together, although the detailed mechanisms of efficient Ag presentation via MHC class I and the maturation and migration of DCs by CT are still unknown, digested OVA might be efficiently captured by immature gut mucosal DCs in the presence of CTB and the captured Ag may be cross-presented by MHC class I during DC maturation and migration in the presence of CTA, resulting in the induction of mucosal class I MHC molecule-restricted CTLs that may cause the regression of previously established tumors.

OVA-specific $CD8^+$ CTLs were induced among not only the IELs but also the LPLs of the stomach, small intestine, and large intestine by oral administration of OVA plus CT, a higher percentage of OVA-specific CD8 CTLs was observed in the stomach, small intestine, and large intestine in order, and more specific CTLs were always detected among IELs than among LPLs (Fig. 4, *E* and *F*). Thus, CTLs are much easier to be induced in the upper and more superficial portions of the gastrointestinal tract when Ags are orally administrated with intact CT.

It has been reported that DCs in gastric mucosa are increased in *Helicobacter pylori* (*Hp*)-infected mice and that the response of DCs and T cells to *Hp* Ag is critical for *Hp*-induced gastritis (41). In the present study, Ag-specific CTLs in the stomach might be generated by mucosally activated DCs in the presence of CT and infiltrate-implanted gastric tumor tissues. It is possible that intestinally activated CTLs might migrate to the tumor-implanted stomach, which might also cause CTL infiltration. Actually, such effector CTLs usually express high levels of $\alpha_4\beta_7$ integrin and can home in to the gastric (42), and small and large intestinal mucosa (43) where mucosal addressin cell-adhesion molecule-1 (MadCAM-1), the ligand of $\alpha_4\beta_7$ integrin, is constitutively expressed by post-capillary endothelial cells in small (44, 45) and large intestinal lamina propria (46). Moreover, the number of gastric $\alpha_4\beta_7^{high}$ T cells increased markedly by oral administration of CT in mice (42). It has also been reported that MAdCAM-1 expression is increased in the gastric mucosa after oral administration with cholera vaccine composed of CTB and formalin-inactivated *V. cholerae* (47); therefore, MadCAM-1-expression in gastric mucosa and the recruitment of effector $\alpha4\beta7^{high}$ T cells to gastric mucosa might be enhanced by oral administration of the CT adjuvant and, thus, OVA-specific effector CTLs might efficiently infiltrate the OVA Ag-expressing tumor region in the stomach.

In the present study, we found that the growth of dermally implanted tumors was also suppressed by the oral administration of tumor Ag plus whole intact CT. The actual mechanisms for such suppression remains to be elucidated, but there are at least three distinct possibilities: first, the migration of Ag-specific CTLs from the gastrointestinal tract to the skin; second, the migration of Ag-presenting DCs activated in the mucosal compartments by CT; and third, the migration of both cells from the gastrointestinal tract to the skin at the same time. It has been reported that the levels of CCR4 expression, which is associated with T cell homing to the skin, are increased in gastric T cells by infection with *Hp* in humans (48). Moreover, mucosal DCs that take up Ag might migrate to regional lymph nodes near the dermal tumor and prime the CTLs there, and the CTLs could effectively infiltrate dermal tumor tissue. Indeed, Belyakov et al. demonstrated an opposite mechanism in which skin-derived DCs containing heat-labile enterotoxin of *Escherichia coli* migrated to PPs and induced mucosal CTLs by transcutaneous immunization of an Ag and CT (49). Although the detailed mechanisms of this migration of DCs between skin and mucosa are unknown, they have clearly shown that DCs can migrate between the mucosa and skin. We are currently comparing the alteration of DCs in the mucosal compartment, spleen, and lymph nodes after oral administration of an Ag plus natural CT.

Unfortunately, such natural CT is not an appropriate mucosal adjuvant for human clinical investigation (50); however, studies

using natural CT would provide important and critical information about the effect of CT that would be useful for mucosal immune activation. Based on the findings obtained by using natural CT in a mouse model system, we could establish much safer protocols with a mutant CT (51) that induces adenosine diphosphate ribosylation and cyclic adenosine monophosphate formation, which may prevent severe diarrhea as well as retain adjuvant properties. Taken together, an artificial CT-based vaccine targeting DCs may provide a strategy for efficient CTL induction and avirulent mucosal cancer vaccination.

Our data also indicate that E.G7-OVA tumor growth was suppressed by OVA-specific CTLs but not NK cells (Fig. 7*B*). Vaccination with OVA-CT-pulsed DC protects against E.G7-OVA tumor development in vivo in wild-type, NK-depleted, and CD4-deficient mice but not in CD8-deficient mice (34), indicating that the E.G7-OVA tumor might be controlled by CD8 T cells but not by NK cells or CD4 T cells. In fact, TILs in the suppressed tumor did not show any NK-related cytotoxicity (Fig. 7*B*). Moreover, it has been demonstrated that in vitro pretreatment of NK cells with CT inhibits NK cell killing of tumor (YAC-1 or P815), because G proteins in NK cell membranes are ADP ribosylated with CT and ribosylation inhibits the lysis of tumor cells (52); therefore, NK cells do not seem to be involved in the suppression of E.G7-OVA growth in vivo.

It has been shown that activated CTLs but not naive CTLs can represent antitumor (22) or antivirus (12) responses in vivo. In the present study, already established E.G7 tumor growth can be suppressed only when OVA-specific CTLs that show specific cytotoxicity without requiring in vitro restimulation are induced, particularly in the mucosal compartment. To our knowledge, this is the first demonstration of the visual suppression of already established tumor growth by the simple oral administration of tumor Ag plus mucosal adjuvant. The findings shown in the present study herald a new era for cancer immunotherapy.

Acknowledgments

We thank Dr. Yoshihiro Kumagai and Yoshihiko Norose for useful discussions and advice.

Disclosures

The authors have no financial conflict of interest.

References

1. Franks, L. M., and M. A. Knowles. 2005. What is cancer? In *Introduction to the Cellular and Molecular Biology of Cancer*, 4th Ed. M. A. Knowles and P. J. Selby, eds. Oxford University Press, New York, pp. 1–24.
2. Finn, O. J. 2003. Cancer vaccines: between the idea and the reality. *Nat. Rev. Immunol.* 3: 630–641.
3. Czerkinsky, C., F. Anjuere, J. R. McGhee, A. George-Chandy, J. Holmgren, M. P. Kieny, K. Fujiyashi, J. F. Mestecky, V. Pierrefite-Carle, C. Rask, and J. B. Sun. 1999. Mucosal immunity and tolerance: relevance to vaccine development. *Immunol. Rev.* 170: 197–222.
4. Yuki, Y., and H. Kiyono. 2003. New generation of mucosal adjuvants for the induction of protective immunity. *Rev. Med. Virol.* 13: 293–310.
5. Takahashi, H. 2003. Antigen presentation in vaccine development. *Comp. Immunol. Microbiol. Infect. Dis.* 26: 309–328.
6. Hayday, A., E. Theodoridis, E. Ramsburg, and J. Shires. 2001. Intraepithelial lymphocytes: exploring the third way in immunology. *Nat. Immunol.* 2: 997–1003.
7. Offit, P. A., and K. I. Dudzik. 1989. Rotavirus-specific cytotoxic T lymphocytes appear at the intestinal mucosal surface after rotavirus infection. *J. Virol.* 63: 3507–3512.
8. Chardes, T., D. Buzoni-Gatel, A. Lepage, F. Bernard, and D. Bout. 1994. *Toxoplasma gondii* oral infection induces specific cytotoxic CD8 $\alpha\beta^+$ Thy-1$^+$ gut intraepithelial lymphocytes, lytic for parasite-infected enterocytes. *J. Immunol.* 153: 4596–4603.
9. Muller, S., M. Buhler-Jungo, and C. Mueller. 2000. Intestinal intraepithelial lymphocytes exert potent protective cytotoxic activity during an acute virus infection. *J. Immunol.* 164: 1986–1994.
10. Taunk, J., A. I. Roberts, and E. C. Ebert. 1992. Spontaneous cytotoxicity of human intraepithelial lymphocytes against epithelial cell tumors. *Gastroenterology* 102: 69–75.
11. Roberts, A. I., S. M. O'Connell, L. Biancone, R. E. Brolin, and E. C. Ebert. 1993. Spontaneous cytotoxicity of intestinal intraepithelial lymphocytes: clues to the mechanism. *Clin. Exp. Immunol.* 94: 527–532.
12. Kuribayashi, H., A. Wakabayashi, M. Shimizu, H. Kaneko, Y. Norose, Y. Nakagawa, J. Wang, Y. Kumagai, D. H. Margulies, and H. Takahashi. 2004. Resistance to viral infection by intraepithelial lymphocytes in HIV-1 P18-I10-specific T-cell receptor transgenic mice. *Biochem. Biophys. Res. Commun.* 316: 356–363.
13. Takahashi, H., J. Cohen, A. Hosmalin, K. B. Cease, R. Houghten, J. L. Cornette, C. DeLisi, B. Moss, R. N. Germain, and J. A. Berzofsky. 1988. An immunodominant epitope of the human immunodeficiency virus envelope glycoprotein gp160 recognized by class I major histocompatibility complex molecule-restricted murine cytotoxic T lymphocytes. *Proc. Natl. Acad. Sci. USA* 85: 3105–3109.
14. Williams, N. A., T. R. Hirst, and T. O. Nashar. 1999. Immune modulation by the cholera-like enterotoxins: from adjuvant to therapeutic. *Immunol. Today* 20: 95–101.
15. Lencer, W. I., and B. Tsai. 2003. The intracellular voyage of cholera toxin: going retro. *Trends Biochem. Sci.* 28: 639–645.
16. Elson, C. O., and W. Ealding. 1984. Generalized systemic and mucosal immunity in mice after mucosal stimulation with cholera toxin. *J. Immunol.* 132: 2736–2741.
17. Marinaro, M., H. F. Staats, T. Hiroi, R. J. Jackson, M. Coste, P. N. Boyaka, N. Okahashi, M. Yamamoto, H. Kiyono, H. Bluethmann, et al. 1995. Mucosal adjuvant effect of cholera toxin in mice results from induction of T helper 2 (Th2) cells and IL-4. *J. Immunol.* 155: 4621–4629.
18. Bowen, J. C., S. K. Nair, R. Reddy, and B. T. Rouse. 1994. Cholera toxin acts as a potent adjuvant for the induction of cytotoxic T-lymphocyte responses with non-replicating antigens. *Immunology* 81: 338–342.
19. Carbone, F. R., and M. J. Bevan. 1989. Induction of ovalbumin-specific cytotoxic T cells by in vivo peptide immunization. *J. Exp. Med.* 169: 603–612.
20. Moore, M. W., F. R. Carbone, and M. J. Bevan. 1988. Introduction of soluble protein into the class I pathway of antigen processing and presentation. *Cell* 54: 777–785.
21. Porgador, A., H. F. Staats, B. Faiola, E. Gilboa, and T. J. Palker. 1997. Intranasal immunization with CTL epitope peptides from HIV-1 or ovalbumin and the mucosal adjuvant cholera toxin induces peptide-specific CTLs and protection against tumor development in vivo. *J. Immunol.* 158: 834–841.
22. Dalyot-Herman, N., O. F. Bathe, and T. R. Malek. 2000. Reversal of CD8$^+$ T cell ignorance and induction of anti-tumor immunity by peptide-pulsed APC. *J. Immunol.* 165: 6731–6737.
23. Eriksson, K., J. B. Sun, I. Nordstrom, M. Fredriksson, M. Lindblad, B. L. Li, and J. Holmgren. 2004. Coupling of antigen to cholera toxin for dendritic cell vaccination promotes the induction of MHC class I-restricted cytotoxic T cells and the rejection of a cognate antigen-expressing model tumor. *Eur. J. Immunol.* 34: 1272–1281.
24. Taguchi, T., J. R. McGhee, R. L. Coffman, K. W. Beagley, J. H. Eldridge, K. Takatsu, and H. Kiyono. 1990. Analysis of Th1 and Th2 cells in murine gut-associated tissues: frequencies of CD4$^+$ and CD8$^+$ T cells that secrete IFN-γ and IL-5. *J. Immunol.* 145: 68–77.
25. Takahashi, M., E. Osono, Y. Nakagawa, J. Wang, J. A. Berzofsky, D. H. Margulies, and H. Takahashi. 2002. Rapid induction of apoptosis in CD8$^+$ HIV-1 envelope-specific murine CTLs by short exposure to antigenic peptide. *J. Immunol.* 169: 6588–6593.
26. Semple, J. W., and M. R. Szewczuk. 1986. Natural killer cells in murine muscular dystrophy: IV. Characterization of Percoll fractionated splenic and thymic natural killer cells and natural killer-sensitive thymocyte targets. *Clin. Immunol. Immunopathol.* 41: 116–129.
27. Belz, G. T., W. Xie, and P. C. Doherty. 2001. Diversity of epitope and cytokine profiles for primary and secondary influenza a virus-specific CD8$^+$ T cell responses. *J. Immunol.* 166: 4627–4633.
28. Nakatsuka, K., H. Sugiyama, Y. Nakagawa, and H. Takahashi. 1999. Purification of antigenic peptide from murine hepatoma cells recognized by class-I major histocompatibility complex molecule-restricted cytotoxic T-lymphocytes induced with B7-1-gene-transfected hepatoma cells. *J. Hepatol.* 30: 1119–1129.
29. Kilshaw, P. J., and K. C. Baker. 1988. A unique surface antigen on intraepithelial lymphocytes in the mouse. *Immunol. Lett.* 18: 149–154.
30. Russell, G. J., C. M. Parker, K. L. Cepek, D. A. Mandelbrot, A. Sood, E. Mizoguchi, E. C. Ebert, M. B. Brenner, and A. K. Bhan. 1994. Distinct structural and functional epitopes of the α E β 7 integrin. *Eur. J. Immunol.* 24: 2832–2841.
31. Lefrancois, L., T. A. Barrett, W. L. Havran, and L. Puddington. 1994. Developmental expression of the α IEL β 7 integrin on T cell receptor γ δ and T cell receptor α β T cells. *Eur. J. Immunol.* 24: 635–640.
32. Rocha, B., P. Vassalli, and D. Guy-Grand. 1994. Thymic and extrathymic origins of gut intraepithelial lymphocyte populations in mice. *J. Exp. Med.* 180: 681–686.
33. Wakabayashi, A., Y. Kumagai, E. Watari, M. Shimizu, M. Utsuyama, K. Hirokawa, and H. Takahashi. 2006. Importance of gastrointestinal ingestion and macromolecular antigens in the vein for oral tolerance induction. *Immunology* 119: 167–177.
34. Sun, J. B., K. Eriksson, B. L. Li, M. Lindblad, J. Azem, and J. Holmgren. 2004. Vaccination with dendritic cells pulsed in vitro with tumor antigen conjugated to cholera toxin efficiently induces specific tumoricidal CD8$^+$ cytotoxic lymphocytes dependent on cyclic AMP activation of dendritic cells. *Clin. Immunol.* 112: 35–44.